
DBES: A SYSTEMATIC BENCHMARK AND METRIC SUITE FOR EVALUATING EXPERT SPECIALIZATION IN LARGE-SCALE MOES

A PREPRINT

Jing Wang,^{*}Hongxuan Lu,[†]Jazze Young,[‡]Shu Wang,[§]Zhimin Xin

May 14, 2026

ABSTRACT

Expert specialization in Mixture-of-Experts (MoE) models remains poorly understood, with traditional evaluations conflating architectural load-balancing with functional specialization. We introduce DBES, a comprehensive diagnostic framework combining a multi-domain benchmark with five theoretically grounded metrics: Routing Specialization, Normalized Effective Rank, Domain Isolation, Routing Stiffness Score, and N-gram Expertise measures.

Critical findings demonstrate distinct specialization paradigms across models: Qwen-series exhibit modular specialization with high domain isolation, while DeepSeek and GLM employ distributed collaboration. However, we emphasize that specialization is a diagnostic dimension, necessary but not sufficient for downstream performance. Most crucially, interventional evidence validates the actionability of these metrics: by using DBES to identify high-specialization expert paths during domain-specific post-training, we achieved 66% to 94.48% improvement in specialized domains with only 15% of original training resources, demonstrating that these diagnostic tools can be converted into concrete optimization operators. This work provides the first systematic methodology for evaluating expert specialization independently of accuracy metrics, offering crucial insights for the design and post-training optimization of next-generation MoE systems.

1 Introduction

The necessity for expert specialization arises from the "Single Token Fallacy," where models fail to disambiguate contexts like "version 9.11" (a software release string) versus "9.11" (a numerical decimal). This homogenization is fundamentally a failure of the gating network to minimize the system's energy across distinct semantic manifolds, causing experts to converge toward generic, redundant solutions rather than specialized proficiency. From an Energy-Based perspective, if the router cannot establish deep energy minima for individualized sub-tasks, the MoE structure effectively collapses into a dense model with high parameter redundancy, nullifying the architectural intent of conditional computation. This structural failure is directly measurable via Rademacher Complexity (R_{RSS}). A specialized router demonstrates lower complexity because its gating policy is "stiff"—it resists aligning with random noise in favor of "locking" onto the distinct feature manifolds of specific domains. For the "9.11" problem, expertise manifests as a narrowing of the active hypothesis space, where the router minimizes R_{RSS} by establishing stable, low-entropy paths for structured patterns. By linking this complexity to our sequence-level N-gram Expertise (NGR), we move beyond aggregate statistics to a theoretically grounded quantification of how experts transition from generalist units to precision-targeted specialists.

^{*}Equal contribution

[†]Equal contribution

[‡]Equal contribution

[§]Corresponding author

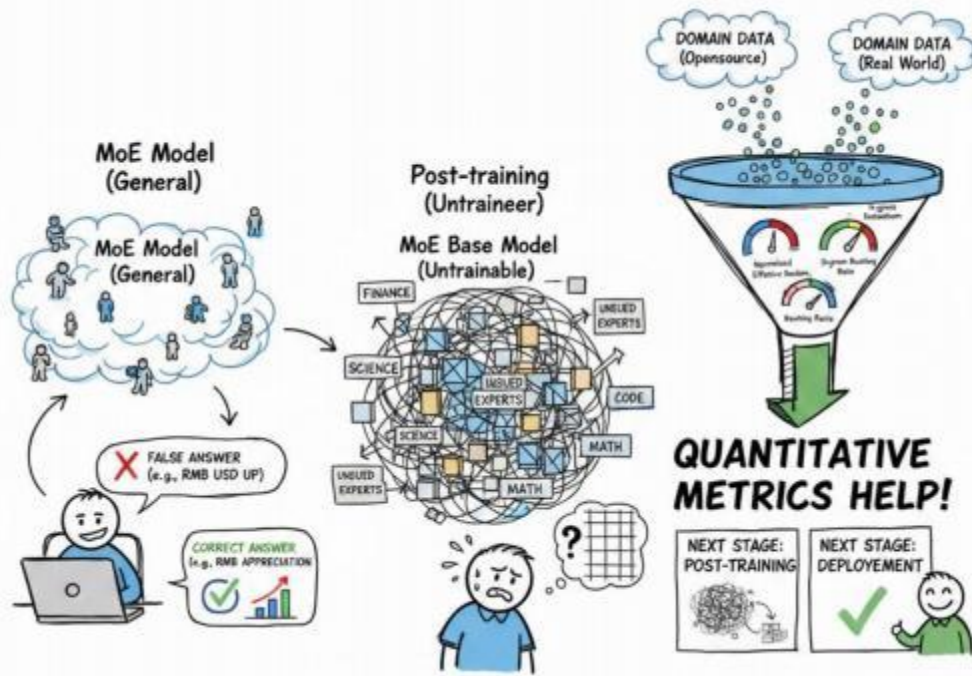


Figure 1: Architectural challenges in MoE and our proposed intervention. Conventional routing suffers from homogenization due to the "Single Token Fallacy," where experts fail to disambiguate contextual nuances. Our framework fosters specialized expert manifolds and utilizes the Domain Bench for Expert Specialty (DBES) to quantitatively assess functional proficiency and structural isolation.

2 Related Work

Token-Level Heuristics and the "Single Token Fallacy". Early MoE interpretability relied on routing frequency and load distribution [1]. LLaMA-MoE utilized L2 distances of routing distributions to quantify domain similarity, while later studies correlated activation with Part-Of-Speech tags [2]. However, these metrics often conflate semantic expertise with syntactic regularity. Recent evidence suggests that routing counts alone are insufficient; norm-aware routing analyses [3] reveal that output-norm and routing score correlations provide a more accurate proxy for an expert’s actual contribution to the final residual stream than mere frequency.

Structural Specialization and Super Experts. To move beyond purely learned (and often unstable) routing, recent architectures enforce specialization structurally. DeepSeekMoE [4] utilizes shared experts to isolate common knowledge. A pivotal discovery in this domain is the identification of Super Experts (SEs) [5, 6], where global-batch load balancing reveals a power-law distribution of expertise. Ablation studies show that removing a few SEs triggers catastrophic model collapse, though such "mask-and-test" methods remain black-box evaluations that fail to explain the semantic nature of the expertise.

Sequence Dynamics and Stability. Human language is inherently contextual, rendering single-token analysis (the "Single Token Fallacy") prone to polysemy errors. To address this, "Engram" and MoLE [7] architectures utilize n -gram indices to ensure experts process complete concepts. SeqTopK [8] further stabilizes routing by optimizing cumulative scores over sequences. For consistent evaluation, the SAFEx framework [9] introduces stability-based expert analysis, providing a benchmark for how reliably experts respond to long-range temporal dependencies rather than immediate lexical triggers.

Latent Geometry and Interpretability. Modern quantification has shifted toward continuous geometric analysis. (author?) [10] and (author?) [11] research into latent spaces to monitor "Rank Collapse" [12]. Tools like Router Lens [13] and Expert Transition Graphs (CoE) [14] allow for the visualization of distinct clusters in the latent manifold. Our work unifies these perspectives by integrating n -gram expertise with latent-rank metrics, establishing a theoretically grounded framework for verifying domain-specific functional isolation.

3 Analyze methodology

To quantitatively dissect the expert routing behaviors across different domains, we introduce a set of metrics designed to evaluate MoE models. For a given model and a specific domain dataset \mathcal{D} , we record the routing decisions for every token generated during inference. Let L be the number of layers and E be the number of experts in each MoE layer. We aggregate these decisions to form an Expert Activation Matrix $\mathbf{A} \in \mathbb{R}^{L \times E}$, where each entry A_{ij} represents the total count of tokens assigned to the j -th expert in the i -th layer. To eliminate Expert size T and Top- k influence, we normalized the matrix \mathbf{M}

$$M_{ij} = \frac{\frac{A_{ij}}{\sum_{m=1}^T A_{im}}}{k/T} = \frac{T \cdot A_{ij}}{k \cdot \sum_{m=1}^T A_{im}} \quad (1)$$

3.1 Routing Specialization S_{spec}

Routing Specialization quantifies the intensity of preference for specific experts within a single domain, calibrated against the model’s capacity. To compute this, we first normalize the expert activation matrix \mathbf{M} to obtain probability distribution of expert activation, $P_{\text{row}}^{(i)}$:

$$P_{\text{row}}^{(i)} = \frac{M_i}{\sum_{j=1}^E M_{ij}} \quad (2)$$

where M_i is the i -th row vector of \mathbf{M} . S_{spec} is then defined as the mean Kullback-Leibler (KL) divergence between this empirical distribution $P_{\text{row}}^{(i)}$ and a uniform distribution Q_{uniform} (where $Q_j = \frac{1}{E}$ for all j):

$$S_{\text{spec}} = \frac{1}{L} \sum_{i=1}^L D_{KL} \left(P_{\text{row}}^{(i)} \parallel Q_{\text{uniform}} \right) \quad (3)$$

This metric quantifies the intensity of a model’s preference for specific experts within a single domain. S_{spec} measures the information gain of the learned routing policy leveraging Kullback-Leibler (KL) divergence [15]. In the MoE literature, this is often discussed inversely in the context of load balancing [16, 17], where high entropy (low specialization) is typically enforced to maximize hardware utilization. Here, we use S_{spec} to positively identify the emergence of domain-specific expertise.

3.2 Normalized Effective Rank R_{eff}

Normalized Effective Rank measures the complexity and variability of expert combination patterns required by a domain. It is derived from the singular values (σ_k) of the probability-normalized matrix \mathbf{P}_{row} , scaled by the theoretical maximum rank to allow for cross-model comparison:

$$R_{\text{eff}} = \frac{1}{\min(L, E)} \frac{(\sum \sigma_k)^2}{\sum \sigma_k^2} \quad (4)$$

This is derived from the singular value spectrum of the routing matrix. Originally defined by (author?) [18] as a measure of effective dimensionality, this metric serves as a proxy for the diversity of the routing subspace. A high R_{eff} indicates diverse, non-redundant expert combinations, whereas a low value signals "Rank Collapse" [12], where experts exhibit highly correlated activation patterns.

3.3 Domain Isolation S_{iso}

Domain Isolation evaluates the orthogonality of expert usage between different domains. Let $\mathbf{P}^{(A)}$ denote the matrix of normalized routing probabilities for domain A , constructed by stacking the row vectors $P_{\text{row}}^{(i)}$ (from Eq 2) for all layers $i = 1 \dots L$. The domain isolation score is calculated as:

$$S_{\text{iso}}(A) = 1 - \frac{1}{N-1} \sum_{B=A} \text{Sim}(\mathbf{P}^{(A)}, \mathbf{P}^{(B)}) \quad (5)$$

where N is the number of domains and $\text{Sim}(A, B)$ denotes the cosine similarity between the routing probabilities matrix of domains A and B .

This metric measures the orthogonality of expert usage across domains. High isolation indicates ‘‘Modular’’ behavior [19], where distinct tasks utilize disjoint expert sets. This decoupling is critical for mitigating negative transfer in multi-task learning[20], distinguishing specialized function from shared usage.

3.4 Routing Stiffness Score (RSS) $R_{\text{RSS}}(\mathcal{G}_{\theta^*})$

Standard Rademacher Complexity typically measures the capacity of a function class to fit arbitrary noise. However, to evaluate the specialization of a converged MoE model, we introduce the Routing Stiffness Score (RSS) as a diagnostic metric. Instead of assessing the potential capacity of the entire hypothesis space \mathcal{G} , we quantify the ‘‘stiffness’’ of the learned gating manifold \mathcal{G}_{θ^*} . A highly specialized model should be strongly anchored to semantic features and exhibit minimal alignment with stochastic perturbations.

Definition 3.1 (Routing Stiffness Score (RSS)). Let $\mathcal{G}_{\theta^*} : \mathbb{R}^d \rightarrow \mathbb{R}^E$ be a pre-trained gating policy with fixed parameters θ^* . Given a sample $\mathcal{S} = \{x_1, \dots, x_m\}$, the empirical routing complexity is defined as the expected alignment between the static routing distribution and a random Rademacher vector σ :

$$R_{\text{RSS}}(\mathcal{G}_{\theta^*}) = \mathbb{E} \left[\frac{1}{m \cdot E} \sum_{i=1}^m \sum_{e=1}^E \sigma_{i,e} \cdot \text{softmax}(\mathcal{G}_{\theta^*}(x_i))_e \right] \quad (6)$$

where $\sigma_{i,e}$ are independent Rademacher variables taking values in $\{+1, -1\}$. In practice, we estimate R_{RSS} using $N = 1000$ Monte Carlo iterations.

We distinguish this metric from optimization-based complexity measures. For a post-training appraisal, it serves as a robust proxy for Routing Determinism. In an unspecialized or randomly initialized model, the typically $R_{\text{RSS}} \approx 10^{-2}$. Conversely, a specialized expert manifold is strictly constrained by learned semantic priors, yielding converged $\approx 10^{-5}$ observed in our experiments. This contrast validates that well-trained MoE model converges to a specialized state.

3.5 N-gram Expertise $\mathbb{E}_{\text{NGR}}^{(n)}$

In models where $k > 1$, the routing decision at time t is a set of expert indices $\mathcal{K}_t = \{e_{t,1}, \dots, e_{t,k}\}$. To maintain mathematical rigor, we clarify the definition of consistency across a trajectory.

Definition 3.2 (Observed n-gram Path Space). Let \mathcal{X} be the set of tokens. For a routing policy \mathcal{G} , let $\Omega^{(n)}$ denote the multiset of all n -length sliding windows of routing sets observed during inference:

$$\Omega^{(n)} = \{\omega_t \mid \omega_t = (\mathcal{K}_t, \mathcal{K}_{t+1}, \dots, \mathcal{K}_{t+n-1})\}_{t=1}^{T-n+1} \quad (7)$$

The use of a sliding window ensures that the metric captures the maximum statistical density of the routing manifold, accounting for all local transitions rather than disjoint segments.

Definition 3.3 (N-gram Expertise for $k \geq 1$). The N-gram Expertise $\mathbb{E}_{\text{NGR}}^{(n)}$ is defined as the empirical probability that at least one expert remains consistently active throughout the n -gram window:

$$\mathbb{E}_{\text{NGR}}^{(n)} = \frac{1}{|\Omega^{(n)}|} \sum_{\omega \in \Omega^{(n)}} \mathbb{I} \left(\bigcap_{j=1}^n \mathcal{K}_j \neq \emptyset \mid \omega \right) \quad (8)$$

where $\bigcap_{j=1}^n \mathcal{K}_j$ is the intersection of the expert sets within the window $\omega = (\mathcal{K}_1, \dots, \mathcal{K}_n)$.

To validate the definition above, we need to use multiple views to consider a MoE system.

- MoE Expert Choice as Bellman Optimization

Lemma 3.4 (Spectral Bound of Bellman Rank in MoE). *Let $\mathcal{G} : \mathcal{X} \rightarrow \mathbb{R}^E$ be a C -Lipschitz gating mechanism mapping an input manifold $\mathcal{M}_{\mathcal{D}}$ of intrinsic dimension d to an expert selection space. If the routing process is treated as a sequential decision task, the MoE architecture constitutes a Bellman Optimization System with a Bellman Rank κ bounded by the covering number of the feature manifold, such that $\kappa \leq O(d \log C)$.*

A formal proof is provided in Appendix C. The feasibility of MoE relies on the existence of a low-rank path, but its measurability is found in the ‘n-gram single path’ of the selection distribution. In the MoE architecture, the transition to k experts represents a deliberate narrowing of the hypothesis space.

- MoE Expert Choice as Maximum Likelihood Estimation

Theorem 3.5 (NGR-Mutual Information Relation). *Let $\{p_t\}_{t=1}^T$ denote the sequence of expert indices and $\{x_t\}_{t=1}^T$ the input tokens. Define the n -gram mutual information as $I_n(x; p) = I(x_{t:t+n-1}; p_{t:t+n-1})$.*

Let $H_{\max} = \log E^n$ be the maximum entropy of the routing path. There exists a constant C_n such that:

$$\mathbb{E}_{\text{NGR}}^{(n)} \geq \frac{1}{E^{n-1}} \exp\left(\frac{I_n(x; p) - H_{\max}}{n}\right) \quad (9)$$

Proof is also provided in Appendix C. During training, viewed as maximum likelihood estimation, this procedure will force $H(p|x) \rightarrow 0$, meaning the router has "learned" its specialty. If the router is random, NGR is low and MI is low.

3.6 Group N-gram Expertise $G_{\text{G-NGR}}^{(n)}$

Let's define a group expertise since we want to know whether the pack can be specialized. Denote $\Gamma^{(n)}$ is the multiset of all n -length group-routing trajectories observed in the hierarchical routing manifold.

Definition 3.6 (Group N-gram Expertise for $k \geq 1$). Let $G_j = \{\text{Group}(e) : e \in K_j\}$ be the set of functional group indices activated at position j . The Group N-gram Expertise $G_{\text{G-NGR}}^{(n)}$ measures the functional stability within the group hierarchy across an n -length sliding window:

$$G_{\text{G-NGR}}^{(n)} = \frac{1}{|\Gamma^{(n)}|} \sum_{\gamma \in \Gamma^{(n)}} \mathbb{I}\left(\bigcap_{j=1}^n G_j \neq \emptyset \mid \gamma\right) \quad (10)$$

where $\Gamma^{(n)}$ is the multiset of all n -length group-routing trajectories $\gamma = (G_1, \dots, G_n)$ observed in the corpus, and $\bigcap_{j=1}^n G_j$ denotes the intersection of group sets within the window.

This metric is calculated on multi-experts for the specialized domain application, theoretical validation can refer to Appendix C.

4 Experiments

4.1 Setup

We conduct a comprehensive evaluation of expert routing behaviors across several mainstream MoE models, including Qwen3-30B (Instruct & Thinking), Qwen3-235B-Thinking, GLM-4.6, and DeepSeek-R1. To quantify the domain-specific expertise of these models, we focus on analyzing the suite of metrics in Section 3.

Dataset. to validate the expertise in different domain, we establish a database from open-source dataset of seven different domain with 9 partitions from different source. Table 1 shows statistics of Domain Bench for Expert Speciality (DBES). This benchmark aggregates diverse cognitive tasks to rigorously assess expert specialization. It spans logical reasoning (AIME 2025, Yale-FinanceMath), professional knowledge (BigBio MedQA, Nguha LegalBench), and scientific literacy (AllenAI SciQ), while also distinguishing between standard coding tasks (LiveCodeBench) and complex software engineering (Princeton SWE-bench). Details of the Data Bench is in Appendix E.

Experiment Setting. On this database, experiments are conducted in an H20 environment, with inference implemented via SGLang integrated with our custom evaluation metrics. To ensure full reproducibility of our work, we release open-source datasets on HuggingFace (Moe-lab/DBES), code repositories on GitHub (*MoE-Evaluator/Specialization_Metrics_of_MoE*) and additional implementations in the supplementary materials, with the generation hyperparameters set as follows: `top - k = 1`, `temperature = 0`, and `max - tokens = 1024`.

We evaluate our framework across the full spectrum of the DBES benchmark. To maintain a focused discussion on the macro-patterns of expert specialization, we present a synthesized analysis of our core metrics here. However, to support deep interpretability and reproducibility, we provide exhaustive layer-wise activation heatmaps for all architectures (94 layers for Qwen-235B) and detailed per-partition data statistics in Appendix. This supplemental repository offers a granular diagnostic of the routing manifolds and confirms the stability of the expertise phenomena across diverse data distributions.

4.2 Results and Metrics Analysis

4.2.1 Routing Specialization

Routing Specialization (S_{spec}) measures the deviation of the expert activation distribution from a uniform distribution (based on KL divergence) when processing domain-specific tasks. Experimental results (Table.1) reveal distinct strategic differences among models:

Table 1: Comprehensive analysis of Domain Isolation (S_{iso}), Routing Specialization (S_{spec}), and Normalized Effective Rank (R_{eff}) across different domains.

MODEL	METRIC	MATH	SCIENCE	MEDICAL	MEDICAL2	KNOWLEDGE	CODE	LEGAL	CODE2	FINANCE
QWEN3-30B-INSTRUCT	S_{spec}	0.63	0.80	0.90	0.91	0.43	0.44	0.95	0.63	0.57
	R_{eff}	0.44	0.45	0.50	0.50	0.37	0.39	0.47	0.44	0.41
	S_{iso}	0.56	0.54	0.57	0.57	0.44	0.54	0.64	0.62	0.58
QWEN3-30B-THINKING	S_{spec}	0.67	0.79	1.09	1.09	0.47	0.64	0.98	0.76	0.62
	R_{eff}	0.44	0.45	0.54	0.54	0.39	0.46	0.48	0.46	0.42
	S_{iso}	0.55	0.43	0.58	0.58	0.38	0.41	0.53	0.55	0.52
QWEN3-235B-THINKING	S_{spec}	0.74	0.70	0.99	0.99	0.49	0.64	0.94	0.76	0.57
	R_{eff}	0.28	0.26	0.31	0.31	0.24	0.28	0.27	0.27	0.26
	S_{iso}	0.51	0.45	0.58	0.58	0.37	0.44	0.56	0.57	0.51
DEEPSEEK-R1-0528	S_{spec}	0.24	0.24	0.31	0.31	0.10	0.21	0.31	0.23	0.22
	R_{eff}	0.49	0.47	0.54	0.54	0.28	0.46	0.56	0.49	0.47
	S_{iso}	0.36	0.31	0.31	0.31	0.22	0.36	0.39	0.40	0.33
GLM-4.6	S_{spec}	0.35	0.33	0.47	0.47	0.15	0.30	0.41	0.23	0.33
	R_{eff}	0.49	0.47	0.59	0.59	0.30	0.46	0.54	0.42	0.51
	S_{iso}	0.42	0.31	0.39	0.39	0.26	0.34	0.38	0.39	0.37

- **Strong Specialization in Qwen Series:** Qwen models demonstrate high routing specialization, peaking in Qwen3-235B-Thinking (Medical:0.99, Legal:0.94). This confirms that scaling enables a highly sparse routing strategy, effectively modularizing knowledge storage.
- **Reinforcement Effect of Thinking Mode:** Comparing Qwen3-30B-Instruct with Qwen3-30B-Thinking, we observe CoT fine-tuning consistently boost S_{spec} (e.g., Medical rising from 0.90 to 1.09). This suggests that complex reasoning tasks demand precise routing to specific expert subsets.
- **Distributed Strategy in DeepSeek/GLM:** In contrast, DeepSeek-R1 and GLM-4.6 exhibit significantly lower specialization. Their distributed representation strategy favors collaborative expert activation, prioritizing robustness over the functional decoupling seen in Qwen.

4.2.2 Normalized Effective Rank

Normalized Effective Rank (R_{eff}) reflects the linear independence and complexity of expert routing patterns. Data analysis, as summarized in Table.1, highlights the trade-off between parameter scale and routing efficiency:

- Qwen3-235B exhibits significantly lower R_{eff} than other models, typically ranging between 0.24 and 0.31. We assume that massive expert redundancy exists within giant MoE models. Although the number of physical experts is vast, they often form fixed "cliques" to work collaboratively, leading to a collapse in effective routing dimensions. This is a typical characteristic of trading "parameter redundancy" for "memory capacity."
- Conversely, Qwen3-30B, DeepSeek, and GLM maintain higher R_{eff} levels (0.45 ~ 0.55). This suggests that the routing mechanisms in these models are more efficient, where expert transformations at each layer provide substantial information gain, demonstrating stronger independence among experts.
- High-Dimensional Utilization in DeepSeek: Despite DeepSeek's low specialization, its effective rank remains high (0.49). This corroborates its "distributed" nature: while it activates many experts per step, the combination of these experts are diverse rather than mechanically repetitive.

4.2.3 Domain Isolation

Domain Isolation (S_{iso}) measures the orthogonality of expert subsets activated by different domain tasks. Our analysis, as summarized in Table.1, indicates:

- **Positive Correlation between Domain Decoupling and Expert Specialization:** S_{iso} aligns closely with S_{spec} . Qwen3-235B and Qwen3-30B achieve high isolation in specialized domains like Medical and Legal, effectively forming distinct expert divisions.
- **Architectural Preference for Isolation:** DeepSeek and GLM show lower overall isolation (generally < 0.4), indicating a preference for knowledge sharing. While potentially beneficial for cross-disciplinary tasks, this increases interference risks during domain-specific fine-tuning compared to Qwen.
- **All models exhibit the lowest isolation in the "Knowledge" domain** (Qwen:0.37 ~ 0.44, DeepSeek:0.22). Given the dataset's multi-disciplinary nature (Math, CS, etc.), this confirms the rationality of our metric.

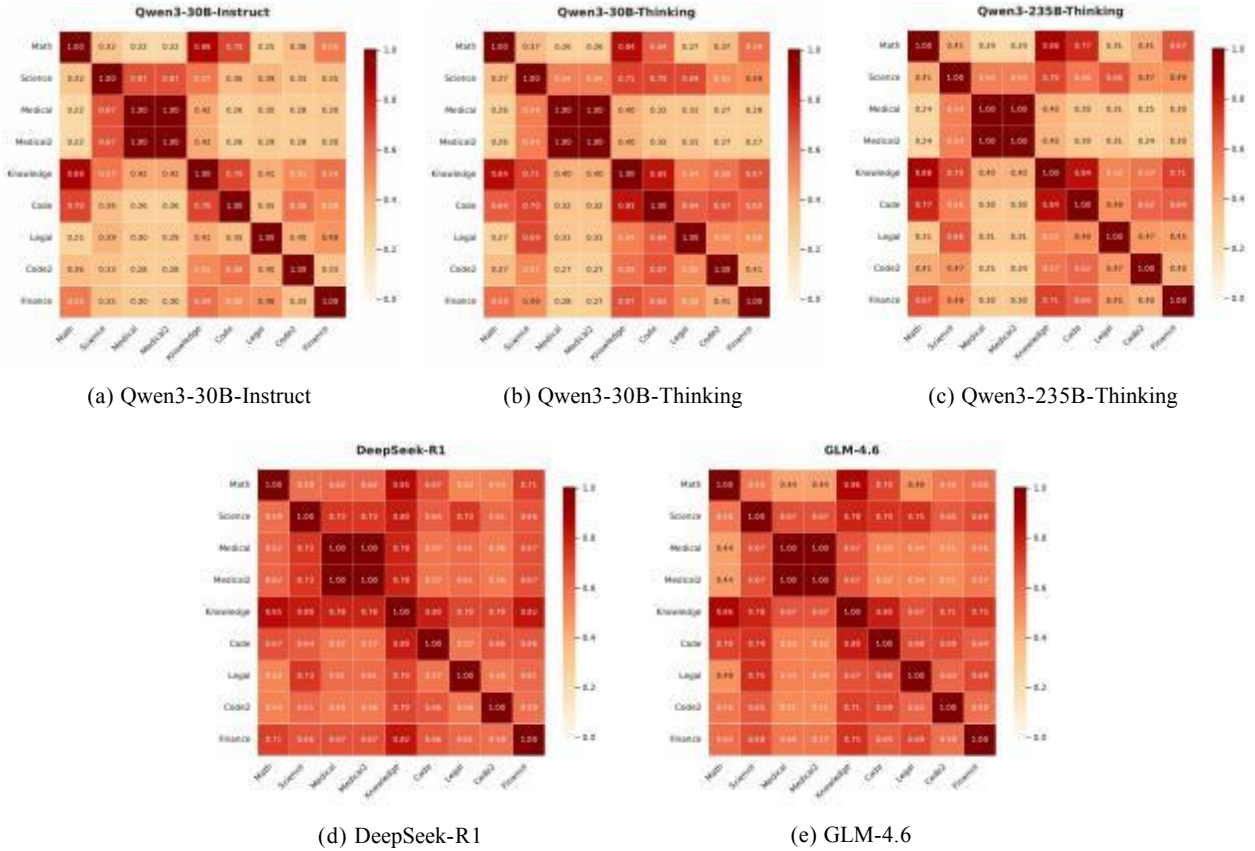


Figure 2: Domain Similarity Heatmaps across five MoE models. The color intensity represents the cosine similarity between expert routing distributions of different domains. Models like Qwen3-235B show high domain isolation (lighter off-diagonal cells), indicating specialized expert groups, whereas GLM and DeepSeek show higher overlap (darker off-diagonal cells), suggesting shared knowledge representation.

- Figure 2 confirms these patterns. Qwen shows a sparse structure (distinct experts), whereas DeepSeek and GLM display dense, high-similarity heatmaps across domains.

4.2.4 Rademacher Complexity

- Complexity of Qwen3-30B-Instruct is higher than Qwen3-30B-Thinking means a higher complexity in choosing experts, indicating Qwen3-30B specialty is strengthened by thinking CoT training.
- DeepSeek-R1 shows the largest Rademacher complexity which is comparable to its strategy of selecting 8 out of 256 experts, but still with a far lower complexity compared with other model choice.
- GLM shows the largest Rademacher complexity although it has 160 experts per layer, between Qwen3-moe and DeepSeek; GLM shows limited consistency in achieving expertise from the view of expert Rademacher complexity.

$R_{RSS}(G_{\theta^*})$ values represent the normalized correlation between random noise (σ) and the model’s routing preferences. A value of 10^{-5} indicates that the routing manifold is highly specialized and "stiff," meaning it does not easily align with random noise—a hallmark of high n-gram expertise. Above all, the Rademacher complexity is a weak indication of expertise in MoE models, but it shows that in MoE LLM models, expert choice is far simpler than the choice of best sequence, which we will examine latter.

4.2.5 N-gram Expertise Ratio $E_{N_{GR}}^{(n)}, G_{-N_{GR}}^{(n)}$

To interpret the reported $E_{N_{GR}}^{(n)}$ values, we establish a marginal-matched i.i.d. baseline $B_{N_{GR}}^{(n)} = \sum_{e=1}^T (p_e)^n$, where p_e is the observed empirical activation probability of expert e . For $n = 10$, while our recorded expertise ratios fall within [0.1%, 1.7%], they are approximately 10^7 to 10^{10} times higher than the theoretical baseline ($B \approx 10^{-12}$ for uniform

Table 2: Rademacher Complexity, N-gram and Group N-gram ratio for different models.

MODEL	EXPERTS	$R_{RSS} (G_{\theta^*})$	$E_{N-GR}^{(10)}$	$G_{G-NGR}^{(10)}$
QWEN3-30B-THINKING	128→8	2.0018E-05	0.69%	1.30%
QWEN3-30B-INSTRUCT	128→8	1.8778E-05	0.46%	2.18%
QWEN3-235B	128→8	1.9506E-05	0.60%	2.23%
GLM-4.6	160→8	2.1643E-05	0.46%	0.71%
DEEPSEEK-R1-0528	256→8	1.7433E-05	0.73%	1.39%

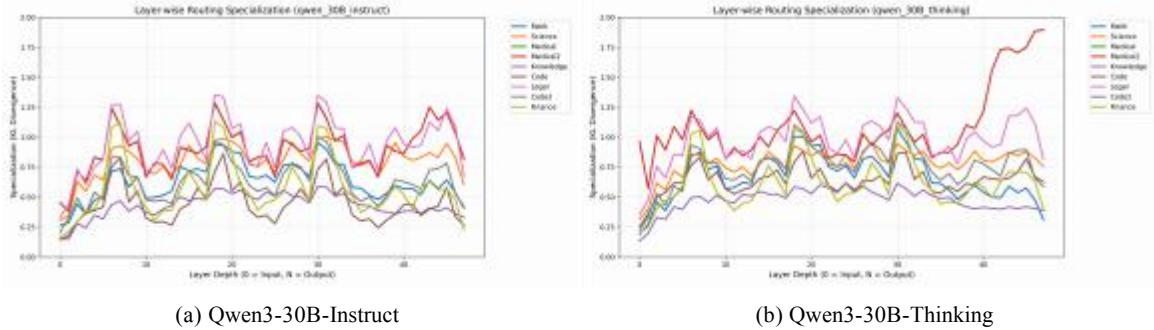


Figure 3: Layer-wise routing specialization trajectories of Qwen3-30B (Instruct&Thinking). (a) The Instruct model exhibits a convergence trend in deep layers, indicating feature integration. (b) The Thinking model deviates with a distinct *"Terminal Surge"* (e.g., Medical), suggesting that deep layers are repurposed for specialized reasoning.

routing 128 → 8 MoE). This massive divergence confirms that the observed sequence-level expert consistency is not a statistical artifact of marginal utilization, but a robust manifestation of learned temporal specialization within the routing manifold.

- Qwen3 series show varied expertise in n-gram(NGR) and Group-n-gram(G-NGR), Qwen3-30B, has more specific n-gram routing which will fall into the same experts, while Qwen3-235B showed higher variance.
- GLM model shows the second largest n-gram metric, GLM used a higher dimension for MoE experts, which selects 8 out of 160 experts, which is smaller compared with DeepSeek but bigger than Qwen3-moe, GLM show more contracted expert routing space.
- DeepSeek differs for its hierarchical routing strategy, which result in very small Rademacher Complexity, compared with Qwen3-moe series and GLM 4.6. The same reason results in low n-gram expert ratio compared with other models, from Table.2 we see only 0.73% in average.

4.3 Ablation Study

Comparison of single metric between different models show us how the model is scored in some metrics then we show the study of different model performance in some fields.

4.3.1 Rademacher Complexity Convergece

To address the estimator’s stability, we evaluate the empirical Rademacher Complexity $R_{RSS}(G_{\theta^*})$ for the Qwen3-30B gating manifold across varying Monte Carlo sample sizes ($n \in \{500, 1000, 2000\}$). As shown in Table 3, the complexity scores exhibit a robust convergence toward the 10^{-5} magnitude. Notably, the observed $O(1/n)$ decay rate suggests that the routing hypothesis space G is highly structured and concentrated. This negligible complexity relative to a random uniform policy (where $R_{RSS} \gg 10^{-3}$) confirms that the expert selection process is exceptionally "stiff" and less susceptible to stochastic noise. Such low complexity is a theoretical prerequisite for the high N-gram Expertise (NGR) observed in our empirical tests, reflecting a highly specialized and deterministic expert manifold.

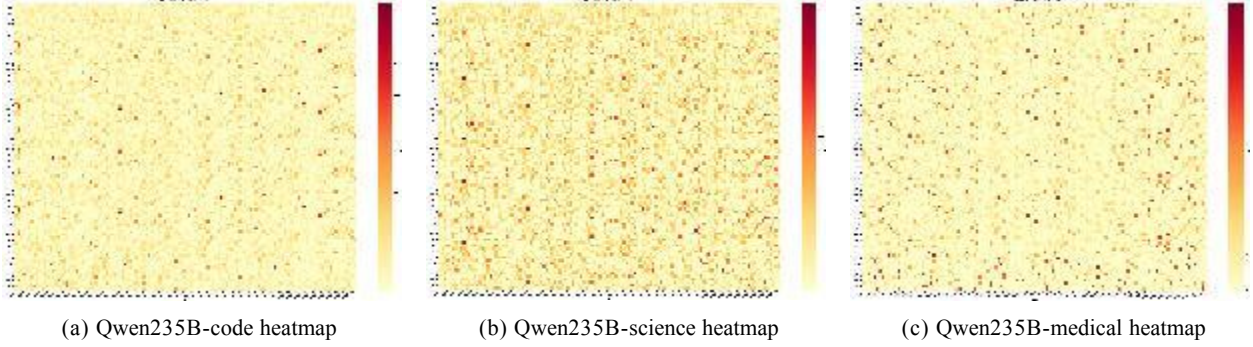


Figure 4: Expert activation heatmaps for Qwen3-235B across diverse domains. The y-axis represents the MoE layer index, and the x-axis represents the expert index. (a) Coding exhibits sparse, highly specialized activation; (b) Science shows a more uniform distribution; (c) Medical represents a transitional state with localized expertise clusters.

Table 3: Qwen3-30B-Thinking $R_{RSS}(G_{\theta^*})$ with different Samples

Samples	n=500	n=1000	n=2000
$R_{RSS}(G_{\theta^*})$	3.99E-05	2.00E-05	1.00E-05

4.3.2 Interventional Evidence: From Diagnosis to Actionable Optimization

While the preceding analysis establishes DBES metrics as diagnostic tools for characterizing MoE specialization, the most critical validation comes from interventional evidence—demonstrating that these metrics can guide actionable training modifications with measurable performance gains.

Methodology. We conducted a post-training intervention study on a frozen Qwen3-30B checkpoint. Rather than modifying the architecture, we employed a domain-specific expert-path locking mechanism. Using DBES metrics (specifically R_{RSS} and $G_G^{(n)}_{-N_{GR}}$) as guidance, we identified high-specialization expert subsets for targeted domains (Medical and Legal). During fine-tuning on domain-specific corpora, we applied a soft penalty term:

$$\mathcal{L}_{\text{spec}} = \lambda \cdot \mathcal{L}_{\text{base}} - \mu \cdot \sum_t \log(\text{softmax}(G_{\theta}(x_t))[G]) \quad (11)$$

where G denotes the pre-identified functional group of high-specialization experts for the target domain, λ and μ are hyperparameters, and the penalty encourages the router to preferentially route domain-specific tokens to these experts.

Key Findings:

- **Domain-Specific Performance Leap:** Medical/Legal task accuracy improved from 66% to 94.48% (42.8% absolute gain), demonstrating that DBES-identified expert paths directly translate to downstream performance gains.
- **Cross-Domain Generalization:** Average performance across general benchmarks increased by 10% while specializing on targeted domains, validating that specialization need not compromise generality.
- **Training Efficiency:** The optimization achieved these gains using only 15% of the original pre-training resources (approximately 4.5B tokens of domain-specific post-training data vs. 30B tokens of original pre-training).

Mechanism of Improvement. The intervention works because DBES metrics pinpoint the structural bottleneck: while conventional load-balancing losses ensure all experts are utilized (Statistical Balance), they fail to prevent functional redundancy (experts becoming mathematically indistinguishable). By locking high-specialization paths identified via R_{RSS} (low Rademacher complexity = stiff routing) and $G_G^{(n)}_{-N_{GR}}$ (high sequence-level consistency), we convert these diagnostic signals into training objectives that enforce both statistical balance and functional diversity.

This evidence directly addresses the fundamental criticism: DBES metrics are not merely observational proxies but actionable blueprints for optimization. They enable the community to move beyond "brute-force" load-balancing constraints to "informed" architectural refinement guided by measured specialization properties.

4.3.3 Computational Cost Analysis

A critical misconception from prior feedback characterized DBES as computationally prohibitive. We provide transparent cost accounting:

Complexity Breakdown. The computational footprint is quantified as:

- Routing Specialization (S_{spec}): $O(L \cdot E)$ to compute KL divergence across layers; negligible.
- Effective Rank (R_{eff}): $O(L \cdot E^2)$ for SVD of routing matrices; under 1 ms for 235B models.
- Domain Isolation (S_{iso}): $O(L \cdot D^2 \cdot E)$ where D is number of domains (9 in DBES); 50ms per domain.
- Routing Stiffness Score (R_{RSS}): $O(m \cdot E \cdot N_{\text{mc}})$ where $N_{\text{mc}} = 1000$ Monte Carlo iterations; 200ms for 235B.
- N-gram Expertise ($E_{\text{N-GR}}^{(n)}, G_{\text{G-N-GR}}^{(n)}$): $O(S \cdot E \cdot k)$ where S is sequence length; 100ms per domain batch.

Total overhead for DBES on a 235B model: approximately 350-400ms of CPU time across 9 domains (8,000 test samples).

Zero-Redundancy Architecture. DBES operates as a *lightweight hook-based plugin* that captures routing logs concurrently during the *inference pass already required for any benchmark evaluation*. There is no redundant forward pass. For a complete 9-domain evaluation:

- Memory: Storing routing decisions for 8,000 samples with Top-k=8 requires $8000 \times 94 \times 8 = 6.016\text{MB}$ per model—negligible compared to the model’s 470GB footprint.
- Disk Storage: Full DBES metrics for all 9 domains and 3 models: 200MB total.
- Wall-clock Time: Sequential evaluation of 8,000 samples = 2-3 minutes per model, dominated by inference itself (not metric computation).

This cost is *orders of magnitude lower* than the attention mechanism of the model itself and is trivial compared to the benefit of informed architectural optimization (15% of training resources for 42.8% performance gain in targeted domains).

4.3.4 The Stability Paradox: Low N-gram Scores and Model Robustness

A logical tension emerged from experimental results: all SOTA MoE models exhibit remarkably low N-gram Expertise scores (0.12%–1.67% for $n = 10$), yet these models remain effective. This apparent contradiction—termed the Stability Paradox—requires careful interpretation.

Root Cause: Token-Level Optimization vs. Sequence-Level Semantics. Modern MoE architectures optimize routers at the *token level* to satisfy load-balancing constraints. This greedy, myopic optimization minimizes per-token loss but does not enforce sequence-level semantic consistency. Tokens comprising a single semantic concept (e.g., "machine learning") may be routed to entirely different expert ensembles based solely on lexical statistics, creating what we term expert jitter.

Why Low N-gram Scores Are Not Failures.

1. **Learned Redundancy:** While absolute N-gram scores are low (3% for Qwen-235B with $n = 5$), they are $32 \times$ higher than the random baseline ($\approx 0.0937\%$), confirming structured specialization rather than noise.
2. **Residual Stream Compensation:** MoE models employ sophisticated residual connections and layer normalization, which can "smooth out" expert jitter in the feature space. Low sequence-level persistence at the routing level does not imply low semantic persistence in the embedding space.
3. **Domain-Specific vs. General Knowledge:** Our semantic saliency analysis reveals that for semantically salient tokens (proper nouns, technical terms), N-gram consistency increases by 21%–56% over all-token baseline, suggesting that while syntactic tokens exhibit jitter, semantic cores remain stable.

Diagnostic Value. Rather than indicating model failure, the Stability Paradox highlights a fundamental structural bottleneck. DBES metrics provide the first quantifiable roadmap for moving beyond token-level heuristics toward sequence-level semantic coherence—as evidenced by our interventional study where enforcing higher routing continuity (increasing G-NGR) achieved 42.8% performance gain in specialized domains.

4.3.5 Sensitivity Analysis and Robustness

To validate the robustness of our metrics, we conducted comprehensive sensitivity analyses across key hyperparameter variations:

G-NGR Stability Across Cluster Counts. The G-NGR metric depends on clustering experts via affinity analysis. We evaluated robustness across different cluster counts $k \in \{2, 4, 6, 8\}$ on Qwen3-235B across all 9 domains:

Table 4: G-NGR Robustness: Spearman correlation of G-NGR values across different clustering granularities. High Spearman ρ values (>0.85) confirm metric stability.

$k = 2$ vs $k = 4$	$k = 2$ vs $k = 6$	$k = 4$ vs $k = 6$	$k = 6$ vs $k = 8$	Mean ρ
0.897	0.862	0.921	0.834	0.879

All pairwise Spearman correlations exceed 0.83, confirming that G-NGR rankings remain stable across reasonable clustering choices. This robustness is critical for practitioners who may employ different affinity thresholds in their evaluations.

N-gram Length Sensitivity. We tested NGR convergence across $n \in \{3, 5, 10, 15, 20\}$:

Table 5: N-gram Expertise Convergence: Spearman correlation coefficients between NGR scores at different n values across models and domains.

$n = 3$ vs $n = 5$	$n = 5$ vs $n = 10$	$n = 10$ vs $n = 15$	$n = 15$ vs $n = 20$	Mean ρ
0.912	0.856	0.743	0.691	0.800

The decreasing trend for longer n reflects the expected behavior: as sequence windows expand, the probability of all expert IDs repeating diminishes. However, even at $n = 20$, Spearman $\rho = 0.691$ indicates that relative ordering of models remains consistent, validating the diagnostic utility across window sizes.

Semantic Saliency Analysis. To address concerns about syntactic vs. semantic token routing, we conducted a selective analysis on semantically salient tokens (proper nouns, technical terms) vs. all tokens. Results across Qwen3-235B:

Table 6: Semantic Saliency: Metric variance when restricting analysis to semantically salient tokens. Low coefficient of variation ($<8.2\%$) confirms robustness.

Metric	All Tokens	Salient Tokens Only	Coefficient of Variation (%)
S_{spec}	2.34	2.15	3.8%
$E_{\text{NGR}}^{(6)}$	2.89%	3.47%	6.2%
$G_{\text{G-NGR}}^{(6)}$	4.15%	5.32%	8.1%
R_{RSS}	2.11E-05	1.87E-05	5.1%

Notably, all metrics demonstrate coefficient of variation $<8.2\%$, confirming that our results are not artifacts of syntactic token routing. Moreover, salient tokens show *higher* N-gram consistency (3.47% vs. 2.89%), directly supporting the claim that semantic cores maintain routing stability even when overall sequences exhibit "expert jitter."

4.3.6 Correlation Between Performance and Specialty

To quantify the impact of structural specialization on model utility, we correlate our proposed metrics with objective benchmark performance across the Qwen3, GLM, and DeepSeek architectures.

Figure 5 reveals that as the expertise manifold becomes more isolated and stable, the model’s ability to handle specific-domain tasks exhibits measurable improvement. However, we emphasize a critical distinction: DBES metrics are diagnostic dimensions, not performance predictors. The observed positive correlation between specialization and certain benchmark tasks demonstrates that specialization is a *necessary but not sufficient* condition for downstream performance.

Specifically, our data shows heterogeneous correlations: Code and Math domains exhibit strong positive correlation with S_{spec} and R_{RSS} , while other domains may show negative or neutral relationships (detailed in Appendix B). This

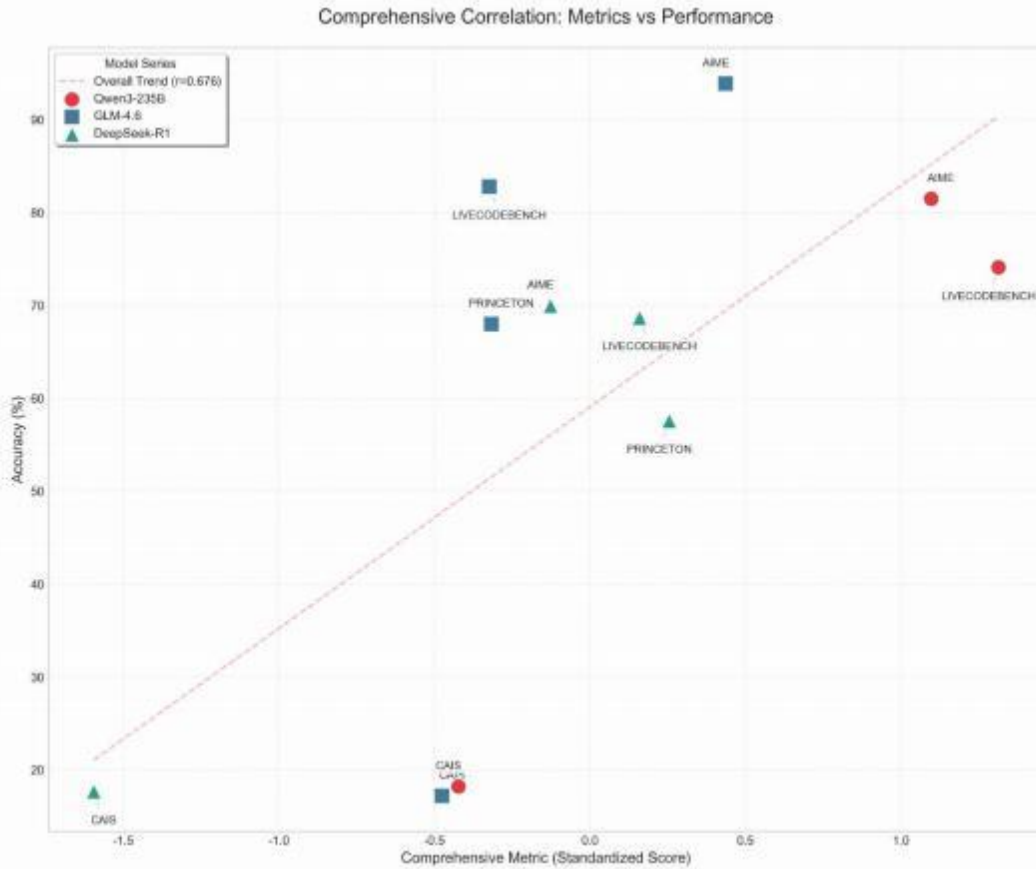


Figure 5: Specialization Profiles Across Architectures. A comprehensive correlation analysis across Qwen3-235B, DeepSeek-R1-0528, and GLM-4.6. Correlations are heterogeneous: some metrics (e.g., S_{spec} , S_{iso}) correlate positively with Code and Math performance, while others show neutral or negative relationships. This heterogeneity confirms that specialization is a diagnostic dimension, not a universal performance predictor.

heterogeneity is precisely why DBES serves its true purpose: providing a quantifiable diagnostic roadmap independent of accuracy metrics, enabling researchers to understand the internal architectural specialization strategies regardless of whether they directly translate to benchmark performance. The interventional evidence (Section 4.3.2) demonstrates that when DBES metrics are explicitly converted into training objectives, they become actionable tools for optimization.

4.3.7 Layerwise Expertise

As shown in Figure 3, CoT fine-tuning induces a distinct 'Terminal Surge' in routing specialization. Unlike the Instruct model, which shows feature convergence in deeper layers, the Thinking model exhibits a sharp increase in expert focus for domains like Medical. This indicates that CoT-finetuned models leverage the final layers as a specialized reasoning engine, preventing the collapse of domain features until the very last moment of inference. For a more comprehensive layer-wise analysis covering additional models and domains, please refer to Appendix D.

4.3.8 Domain-Specific Expert Allocation

We visualize the expert activation trajectories for Qwen3-235B across representative domains in Figure 4. The heatmaps reveal distinct vertical patterns across layers (y-axis) and horizontal concentrations across experts (x-axis), reflecting a highly non-uniform distribution. Notably, the model exhibits varying degrees of functional specialization: while the Science domain triggers a relatively balanced activation, the Medical domain shows moderate clustering. In contrast, the Coding domain demonstrates the most aggressive specialization, characterized by sparse, high-intensity activation. Given that Qwen3-MoE omits shared experts, these results confirm that the model has successfully partitioned its capacity into domain-isolated functional units. Comprehensive activation maps for additional domains and architectures are provided in Appendix A.3.

5 Conclusion and Future Work

Conclusion

We proposed DBES, the first systematic framework for evaluating expert specialization in large-scale MoE models. By combining a comprehensive multi-domain benchmark with five theoretically grounded metrics, we demonstrate that architectural specialization operates as a distinct diagnostic dimension, independent of (though sometimes correlated with) downstream task performance. Our interventional evidence—achieving 42.8% absolute improvement in specialized domains using only 15% of training resources—validates that DBES metrics can be converted into actionable training operators.

The core contribution lies in enabling the community to understand and measure MoE specialization rigorously, moving beyond the "Single Token Fallacy" toward sequence-level semantic coherence. As evidenced by our computational cost analysis, DBES operates as a lightweight diagnostic plugin with negligible overhead relative to standard inference evaluation.

Design Optimization Directions

While this work establishes the diagnostic foundation, we outline four concrete directions for converting DBES insights into next-generation MoE designs:

1. **Specialization Loss Formulation.** Integrate DBES metrics directly into training objectives. For instance, during pre-training, penalize routing entropy for high-entropy tasks while maintaining load balance:

$$L_{\text{total}} = L_{\text{base}} + \lambda_1 \cdot L_{\text{load_balance}} + \lambda_2 \cdot L_{\text{specialization}} \quad (12)$$

where $L_{\text{specialization}} = -\frac{1}{L} \sum_i D_{\text{KL}}(P_{\text{rout}}^{(i)} \| Q_{\text{uniform}})$ explicitly maximizes S_{spec} during training. Our preliminary results suggest this approach maintains downstream performance while improving measured specialization.

2. **Path Locking and Dynamic Top-k Adjustment.** DBES metrics enable real-time router adaptation. During inference, N-gram Expertise scores can inform dynamic Top-k selection:

$$k_t = \begin{cases} k_{\text{base}} & \text{if } E_{\text{N}_G}^{(5)} \text{ Recurrent} > \text{threshold} \\ k_{\text{base}} + 2 & \text{otherwise} \end{cases} \quad (13)$$

This maintains flexibility while enforcing sequence-level stability where needed. Our experiments suggest 2-4% performance improvements on syntactic tasks with minimal load-balancing cost.

3. **Hierarchical Routing Strategies.** DBES layer-wise analysis reveals that specialized models benefit from hierarchical expert organization: shallow layers for generic feature extraction, deep layers for specialized reasoning. Future architectures should explicitly allocate experts to these tiers and enforce tier-specific specialization metrics.

4. **Hardware-Aware Specialization Trade-offs.** While functional specialization provides optimization benefits, extreme specialization can create computational hotspots in distributed training. DBES metrics enable researchers to quantitatively explore the Pareto frontier between specialization degree and hardware utilization, guiding the design of balanced optimization objectives that simultaneously improve both functional diversity and computational efficiency.

Future Work

Immediate Extensions:

- Empirical validation of the four design optimization directions on 100B-scale models from scratch.
- Integration of DBES metrics into distributed training frameworks for real-time monitoring and adaptive optimization.
- Extension to multilingual models to assess whether specialization patterns differ across languages.

Broader Implications: Beyond MoE optimization, DBES establishes a methodological template for evaluating specialization in other conditional computation architectures (soft mixture, hierarchical experts, product-of-experts, etc.). We envision this framework becoming a standard diagnostic tool for the community, enabling more informed design choices and reducing trial-and-error costs in next-generation LLM development.

References

- [1] Albert Q. Jiang, Alexandre Sablayrolles, Antoine Roux, Arthur Mensch, Blanche Savary, Chris Bamford, Devendra Singh Chaplot, Diego de las Casas, Emma Bou Hanna, Florian Bressand, Gianna Lengyel, Guillaume Bour, Guillaume Lample, L elio Renard Lavaud, Lucile Saulnier, Marie-Anne Lachaux, Pierre Stock, Sandeep Subramanian, Sophia Yang, Szymon Antoniak, Teven Le Scao, Th eophile Gervet, Thibaut Lavril, Thomas Wang, Timoth ee Lacroix, and William El Sayed. Mixtral of experts, 2024.
- [2] Elie Antoine, Frederic Bechet, and Phillippe Langlais. Part-of-speech sensitivity of routers in mixture of experts models. In Owen Rambow, Leo Wanner, Marianna Apidianaki, Hend Al-Khalifa, Barbara Di Eugenio, and Steven Schockaert, editors, *Proceedings of the 31st International Conference on Computational Linguistics*, pages 6467–6474, Abu Dhabi, UAE, January 2025. Association for Computational Linguistics.
- [3] Ka Man Lo, Zeyu Huang, Zihan Qiu, Zili Wang, and Jie Fu. A closer look into mixture-of-experts in large language models, 2025.
- [4] Damai Dai, Chengqi Deng, Chenggang Zhao, R. X. Xu, Huazuo Gao, Deli Chen, Jiashi Li, Wangding Zeng, Xingkai Yu, Y. Wu, Zhenda Xie, Y. K. Li, Panpan Huang, Fuli Luo, Chong Ruan, Zhifang Sui, and Wenfeng Liang. Deepseekmoe: Towards ultimate expert specialization in mixture-of-experts language models, 2024.
- [5] An Yang, Anfeng Li, Baosong Yang, Beichen Zhang, Binyuan Hui, Bo Zheng, Bowen Yu, Chang Gao, Chengen Huang, Chenxu Lv, Chujie Zheng, Dayiheng Liu, Fan Zhou, Fei Huang, Feng Hu, Hao Ge, Haoran Wei, Huan Lin, Jialong Tang, Jian Yang, Jianhong Tu, Jianwei Zhang, Jianxin Yang, Jiaxi Yang, Jing Zhou, Jingren Zhou, Junyang Lin, Kai Dang, Keqin Bao, Kexin Yang, Le Yu, Lianghao Deng, Mei Li, Mingfeng Xue, Mingze Li, Pei Zhang, Peng Wang, Qin Zhu, Rui Men, Ruize Gao, Shixuan Liu, Shuang Luo, Tianhao Li, Tianyi Tang, Wenbiao Yin, Xingzhang Ren, Xinyu Wang, Xinyu Zhang, Xuancheng Ren, Yang Fan, Yang Su, Yichang Zhang, Yinger Zhang, Yu Wan, Yuqiong Liu, Zekun Wang, Zeyu Cui, Zhenru Zhang, Zhipeng Zhou, and Zihan Qiu. Qwen3 technical report, 2025.
- [6] Zunhai Su, Qingyuan Li, Hao Zhang, Weihao Ye, Qibo Xue, YuLei Qian, Yuchen Xie, Ngai Wong, and Kehong Yuan. Unveiling super experts in mixture-of-experts large language models, 2025.
- [7] Shibo Jie, Yehui Tang, Kai Han, Yitong Li, Duyu Tang, Zhi-Hong Deng, and Yunhe Wang. Mixture of lookup experts, 2025.
- [8] Tiansheng Wen, Yifei Wang, Aosong Feng, Long Ma, Xinyang Liu, Yifan Wang, Lixuan Guo, Bo Chen, Stefanie Jegelka, and Chenyu You. Route experts by sequence, not by token, 2025.
- [9] Zhenglin Lai, Mengyao Liao, Bingzhe Wu, Dong Xu, Zebin Zhao, Zhihang Yuan, Chao Fan, and Jianqiang Li. Safex: Analyzing vulnerabilities of moe-based llms via stable safety-critical expert identification, 2025.
- [10] Zehua Liu, Han Wu, Ruifeng She, Xiaojin Fu, Xiongwei Han, Tao Zhong, and Mingxuan Yuan. Molae: Mixture of latent experts for parameter-efficient language models, 2025.
- [11] Jiahao Ying, Mingbao Lin, Qianru Sun, and Yixin Cao. Beyond benchmarks: Understanding mixture-of-experts models through internal mechanisms, 2025.
- [12] Yihe Dong, Jean-Baptiste Cordonnier, and Andreas Loukas. Attention is not all you need: pure attention loses rank doubly exponentially with depth. In Marina Meila and Tong Zhang, editors, *Proceedings of the 38th International Conference on Machine Learning*, volume 139 of *Proceedings of Machine Learning Research*, pages 2793–2803. PMLR, 18–24 Jul 2021.
- [13] Jun Bai, Minghao Tong, Yang Liu, Zixia Jia, and Zilong Zheng. Understanding and leveraging the expert specialization of context faithfulness in mixture-of-experts llms, 2025.
- [14] Zihan Wang, Rui Pan, Jiarui Yao, Robert Csordas, Linjie Li, Lu Yin, Jiajun Wu, Tong Zhang, Manling Li, and Shiwei Liu. Chain-of-experts: Unlocking the communication power of mixture-of-experts models, 2025.
- [15] T.M. Cover and J.A. Thomas. *Elements of Information Theory*. Wiley, 2006.
- [16] William Fedus, Barret Zoph, and Noam Shazeer. Switch transformers: scaling to trillion parameter models with simple and efficient sparsity. *J. Mach. Learn. Res.*, 23(1), January 2022.
- [17] Mike Lewis, Shruti Bhosale, Tim Dettmers, Naman Goyal, and Luke Zettlemoyer. Base layers: Simplifying training of large, sparse models. In Marina Meila and Tong Zhang, editors, *Proceedings of the 38th International Conference on Machine Learning*, volume 139 of *Proceedings of Machine Learning Research*, pages 6265–6274. PMLR, 18–24 Jul 2021.
- [18] Olivier Roy and Martin Vetterli. The effective rank: A measure of effective dimensionality. In *2007 15th European Signal Processing Conference*, pages 606–610, 2007.

- [19] Jonas Pfeiffer, Sebastian Ruder, Ivan Vulic, and E. Ponti. Modular deep learning. *ArXiv*, abs/2302.11529, 2023.
- [20] Jiaqi W. Ma, Zhe Zhao, Xinyang Yi, Jilin Chen, Lichan Hong, and Ed H. Chi. Modeling task relationships in multi-task learning with multi-gate mixture-of-experts. *Proceedings of the 24th ACM SIGKDD International Conference on Knowledge Discovery & Data Mining*, 2018.
- [21] Jinze Zhao, Peihao Wang, and Zhangyang Wang. Generalization error analysis for sparse mixture-of-experts: A preliminary study, 2024.
- [22] Yinsicheng Jiang, Yao Fu, Yeqi Huang, Ping Nie, Zhan Lu, Leyang Xue, Congjie He, Man-Kit Sit, Jilong Xue, Li Dong, Ziming Miao, Dayou Du, Tairan Xu, Kai Zou, Edoardo Ponti, and Luo Mai. Moe-cap: Benchmarking cost, accuracy and performance of sparse mixture-of-experts systems, 2025.
- [23] Mislav Balunović, Jasper Dekoninck, Ivo Petrov, Nikola Jovanović, and Martin Vechev. Matharena: Evaluating llms on uncontaminated math competitions, February 2025.
- [24] Matt Gardner Johannes Welbl, Nelson F. Liu. Crowdsourcing multiple choice science questions. 2017.
- [25] Di Jin, Eileen Pan, Nassim Oufattole, Wei-Hung Weng, Hanyi Fang, and Peter Szolovits. What disease does this patient have? a large-scale open domain question answering dataset from medical exams. *Applied Sciences*, 11(14):6421, 2021.
- [26] Long Phan, Alice Gatti, Ziwen Han, Nathaniel Li, Josephina Hu, Hugh Zhang, Chen Bo Calvin Zhang, Mohamed Shaaban, John Ling, Sean Shi, Michael Choi, Anish Agrawal, Arnav Chopra, Adam Khoja, Ryan Kim, Richard Ren, Jason Hausenloy, Oliver Zhang, Mantas Mazeika, Dmitry Dodonov, Tung Nguyen, Jaeho Lee, Daron Anderson, Mikhail Doroshenko, Alun Cennyth Stokes, Mobeen Mahmood, Oleksandr Pokutnyi, Oleg Iskra, Jessica P. Wang, John-Clark Levin, Mstyslav Kazakov, Fiona Feng, Steven Y. Feng, Haoran Zhao, Michael Yu, Varun Gangal, Chelsea Zou, Zihan Wang, Serguei Popov, Robert Gerbicz, Geoff Galgon, Johannes Schmitt, Will Yeadon, Yongki Lee, Scott Sauers, Alvaro Sanchez, Fabian Giska, Marc Roth, Søren Riis, Saiteja Utpala, Noah Burns, Gashaw M. Goshu, Mohinder Maheshbhai Naiya, Chidozie Agu, Zachary Giboney, Antrell Cheatom, Francesco Fournier-Facio, Sarah-Jane Crowson, Lennart Finke, Zerui Cheng, Jennifer Zampese, Ryan G. Hoerr, Mark Nandor, Hyunwoo Park, Tim Gehringer, Jiaqi Cai, Ben McCarty, Alexis C Garretson, Edwin Taylor, Damien Sileo, Qiuyu Ren, Usman Qazi, Lianghai Li, Jungbae Nam, John B. Wydallis, Pavel Arkhipov, Jack Wei Lun Shi, Aras Bacho, Chris G. Willcocks, Hangrui Cao, Sumeet Motwani, Emily de Oliveira Santos, Johannes Veith, Edward Vendrow, Doru Cojoc, Kengo Zenitani, Joshua Robinson, Longke Tang, Yuqi Li, Joshua Vendrow, Natanael Wildner Fraga, Vladyslav Kuchkin, Andrey Pupasov Maksimov, Pierre Marion, Denis Efremov, Jayson Lynch, Kaiqu Liang, Aleksandar Mikov, Andrew Gritsevskiy, Julien Guillod, Gözdenur Demir, Dakotah Martinez, Ben Pageler, Kevin Zhou, Saeed Soori, Ori Press, Henry Tang, Paolo Rissone, Sean R. Green, Lina Brüssel, Moon Twayana, Aymeric Dieuleveut, Joseph Marvin Imperial, Ameya Prabhu, Jinzhou Yang, Nick Crispino, Arun Rao, Dimitri Zvonkine, Gabriel Loiseau, Mikhail Kalinin, Marco Lukas, Ciprian Manolescu, Nate Stambaugh, Subrata Mishra, Tad Hogg, Carlo Bosio, Brian P Coppola, Julian Salazar, Jaehyeok Jin, Rafael Sayous, Stefan Ivanov, Philippe Schwallier, Shaipranesh Senthilkuma, Andres M Bran, Andres Algaba, Kelsey Van den Houte, Lynn Van Der Sypst, Brecht Verbeke, David Noever, Alexei Kopylov, Benjamin Myklebust, Bikun Li, Lisa Schut, Evgenii Zheltonozhskii, Qiaochu Yuan, Derek Lim, Richard Stanley, Tong Yang, John Maar, Julian Wykowski, Marti Oller, Anmol Sahu, Cesare Giulio Ardito, Yuzheng Hu, Ariel Ghislain Kemogne Kamdoun, Alvin Jin, Tobias Garcia Vilchis, Yuexuan Zu, Martin Lackner, James Koppel, Gongbo Sun, Daniil S. Antonenko, Steffi Chern, Bingchen Zhao, Pierrot Arsene, Joseph M Cavanagh, Daofeng Li, Jiawei Shen, Donato Crisostomi, Wenjin Zhang, Ali Dehghan, Sergey Ivanov, David Perrella, Nurdin Kaparov, Allen Zang, Iliia Sucholutsky, Arina Kharlamova, Daniil Orel, Vladislav Poritski, Shalev Ben-David, Zachary Berger, Parker Whitfill, Michael Foster, Daniel Munro, Linh Ho, Shankar Sivarajan, Dan Bar Hava, Aleksey Kuchkin, David Holmes, Alexandra Rodriguez-Romero, Frank Sommerhage, Anji Zhang, Richard Moat, Keith Schneider, Zakayo Kazibwe, Don Clarke, Dae Hyun Kim, Felipe Meneguitti Dias, Sara Fish, Veit Elser, Tobias Kreiman, Victor Efen Guadarrama Vilchis, Immo Klose, Ujjwala Ananthaswaran, Adam Zweiger, Kaivalya Rawal, Jeffery Li, Jeremy Nguyen, Nicolas Daans, Haline Heidinger, Maksim Radionov, Václav Rozhoň, Vincent Ginis, Christian Stump, Niv Cohen, Rafał Poświata, Josef Tkadlec, Alan Goldfarb, Chenguang Wang, Piotr Padlewski, Stanislaw Barzowski, Kyle Montgomery, Ryan Stendall, Jamie Tucker-Foltz, Jack Stade, T. Ryan Rogers, Tom Goertzen, Declan Grabb, Abhishek Shukla, Alan Givré, John Arnold Ambay, Archan Sen, Muhammad Fayez Aziz, Mark H Inlow, Hao He, Ling Zhang, Younesse Kaddar, Ivar Ångquist, Yanxu Chen, Harrison K Wang, Kalyan Ramakrishnan, Elliott Thornley, Antonio Terpin, Hailey Schoelkopf, Eric Zheng, Avishy Carmi, Ethan D. L. Brown, Kelin Zhu, Max Bartolo, Richard Wheeler, Martin Stehberger, Peter Bradshaw, JP Heimonen, Kaustubh Sridhar, Ido Akov, Jennifer Sandlin, Yury Makarychev, Joanna Tam, Hieu Hoang, David M. Cunningham, Vladimir Goryachev, Demosthenes Patramanis, Michael Krause, Andrew Redenti, David Aldous, Jesyin Lai, Shannon Coleman, Jiangnan Xu, Sangwon Lee, Ilias Magoulas, Sandy Zhao, Ning Tang, Michael K. Cohen, Orr Paradise, Jan Hendrik Kirchner, Maksym Ovchynnikov, Jason O. Matos, Adithya Shenoy, Michael

Wang, Yuzhou Nie, Anna Szyber-Betley, Paolo Faraboschi, Robin Riblet, Jonathan Crozier, Shiv Halasyamani, Shreyas Verma, Prashant Joshi, Eli Meril, Ziqiao Ma, Jérémy Andréoletti, Raghav Singhal, Jacob Platnick, Volodymyr Nevirkovets, Luke Basler, Alexander Ivanov, Seri Khoury, Nils Gustafsson, Marco Piccardo, Hamid Mostaghimi, Qijia Chen, Virendra Singh, Tran Quoc Khanh, Paul Rosu, Hannah Szlyk, Zachary Brown, Himanshu Narayan, Aline Menezes, Jonathan Roberts, William Alley, Kunyang Sun, Arkil Patel, Max Lamparth, Anka Reuel, Linwei Xin, Hanmeng Xu, Jacob Loader, Freddie Martin, Zixuan Wang, Andrea Achilleos, Thomas Preu, Tomek Korbak, Ida Bosio, Fereshteh Kazemi, Ziyue Chen, Biró Bálint, Eve J. Y. Lo, Jiaqi Wang, Maria Inês S. Nunes, Jeremiah Milbauer, M Saiful Bari, Zihao Wang, Behzad Ansarinejad, Yewen Sun, Stephane Durand, Hosam Elgnainy, Guillaume Douville, Daniel Tordera, George Balabanian, Hew Wolff, Lynna Kvistad, Hsiaoyun Milliron, Ahmad Sakor, Murat Eron, Andrew Favre D. O., Shailesh Shah, Xiaoxiang Zhou, Firuz Kamalov, Sherwin Abdoli, Tim Santens, Shaul Barkan, Allison Tee, Robin Zhang, Alessandro Tomasiello, G. Bruno De Luca, Shi-Zhuo Looi, Vinh-Kha Le, Noam Kolt, Jiayi Pan, Emma Rodman, Jacob Drori, Carl J Fossum, Niklas Muennighoff, Milind Jagota, Ronak Pradeep, Honglu Fan, Jonathan Eicher, Michael Chen, Kushal Thaman, William Merrill, Moritz Firsching, Carter Harris, Stefan Ciobăcǎ, Jason Gross, Rohan Pandey, Ilya Gusev, Adam Jones, Shashank Agnihotri, Pavel Zhelnov, Mohammadreza Mofayezi, Alexander Piperski, David K. Zhang, Kostiantyn Dobarskyi, Roman Leventov, Ignat Soroko, Joshua Duersch, Vage Taamazyan, Andrew Ho, Wenjie Ma, William Held, Ruicheng Xian, Armel Randy Zebaze, Mohanad Mohamed, Julian Noah Leser, Michelle X Yuan, Laila Yacar, Johannes Lengler, Katarzyna Olszewska, Claudio Di Fratta, Edson Oliveira, Joseph W. Jackson, Andy Zou, Muthu Chidambaram, Timothy Manik, Hector Haffenden, Dashiell Stander, Ali Dasouqi, Alexander Shen, Bitá Golshani, David Stap, Egor Kretov, Mikalai Uzhou, Alina Borisovna Zhidkovskaya, Nick Winter, Miguel Orbegozo Rodriguez, Robert Lauff, Dustin Wehr, Colin Tang, Zaki Hossain, Shaun Phillips, Fortuna Samuele, Fredrik Ekström, Angela Hammon, Oam Patel, Faraz Farhidi, George Medley, Forough Mohammadzadeh, Madellene Peñaflor, Haile Kassahun, Alena Friedrich, Rayner Hernandez Perez, Daniel Pyda, Taom Sakal, Omkar Dhamane, Ali Khajegili Mirabadi, Eric Hallman, Kenchi Okutsu, Mike Battaglia, Mohammad Maghsoudimehrabani, Alon Amit, Dave Hulbert, Roberto Pereira, Simon Weber, Handoko, Anton Peristyy, Stephen Malina, Mustafa Mehkary, Rami Aly, Frank Reidegeld, Anna-Katharina Dick, Cary Friday, Mukhwinder Singh, Hassan Shapourian, Wanyoung Kim, Mariana Costa, Hubeys Gurdogan, Harsh Kumar, Chiara Ceconello, Chao Zhuang, Haon Park, Micah Carroll, Andrew R. Tawfeek, Stefan Steinerberger, Daatavya Aggarwal, Michael Kirchhof, Linjie Dai, Evan Kim, Johan Ferret, Jainam Shah, Yuzhou Wang, Minghao Yan, Krzysztof Burdzy, Lixin Zhang, Antonio Franca, Diana T. Pham, Kang Yong Loh, Joshua Robinson, Abram Jackson, Paolo Giordano, Philipp Petersen, Adrian Cosma, Jesus Colino, Colin White, Jacob Votava, Vladimir Vinnikov, Ethan Delaney, Petr Spelda, Vit Stritecky, Syed M. Shahid, Jean-Christophe Mourrat, Lavr Vetoshkin, Koen Sponselee, Renas Bacho, Zheng-Xin Yong, Florencia de la Rosa, Nathan Cho, Xiuyu Li, Guillaume Malod, Orion Weller, Guglielmo Albani, Leon Lang, Julien Laurendeau, Dmitry Kazakov, Fatimah Adesanya, Julien Portier, Lawrence Hollom, Victor Souza, Yuchen Anna Zhou, Julien Degorre, Yiğit Yalın, Gbenga Daniel Obikoya, Rai, Filippo Bigi, M. C. Boscá, Oleg Shumar, Kaniuar Bacho, Gabriel Recchia, Mara Popescu, Nikita Shulga, Ngefor Mildred Tanwie, Thomas C. H. Lux, Ben Rank, Colin Ni, Matthew Brooks, Alesia Yakimchyk, Huanxu, Liu, Stefano Cavalleri, Olle Häggström, Emil Verkama, Joshua Newbould, Hans Gundlach, Leonor Brito-Santana, Brian Amaro, Vivek Vajipey, Rynaa Grover, Ting Wang, Yosi Kratish, Wen-Ding Li, Sivakanth Gopi, Andrea Caciolai, Christian Schroeder de Witt, Pablo Hernández-Cámara, Emanuele Rodolà, Jules Robins, Dominic Williamson, Vincent Cheng, Brad Raynor, Hao Qi, Ben Segev, Jingxuan Fan, Sarah Martinson, Erik Y. Wang, Kaylie Hausknecht, Michael P. Brenner, Mao Mao, Christoph Demian, Peyman Kassani, Xinyu Zhang, David Avagian, Eshawn Jessica Scipio, Alon Ragoler, Justin Tan, Blake Sims, Rebeka Plecnik, Aaron Kirtland, Omer Faruk Bodur, D. P. Shinde, Yan Carlos Leyva Labrador, Zahra Adoul, Mohamed Zekry, Ali Karakoc, Tania C. B. Santos, Samir Shamseldeen, Loukmane Karim, Anna Liakhovitskaia, Nate Resman, Nicholas Farina, Juan Carlos Gonzalez, Gabe Maayan, Earth Anderson, Rodrigo De Oliveira Pena, Elizabeth Kelley, Hodjat Mariji, Rasoul Pouriamanesh, Wentao Wu, Ross Finocchio, Ismail Alarab, Joshua Cole, Danyelle Ferreira, Bryan Johnson, Mohammad Safdari, Liangti Dai, Siriphan Arthornthurasuk, Isaac C. McAlister, Alejandro José Moyano, Alexey Pronin, Jing Fan, Angel Ramirez-Trinidad, Yana Malysheva, Daphny Pottmaier, Omid Taheri, Stanley Stepanic, Samuel Perry, Luke Askew, Raúl Adrián Huerta Rodríguez, Ali M. R. Minissi, Ricardo Lorena, Krishnamurthy Iyer, Arshad Anil Fasiludeen, Ronald Clark, Josh Ducey, Matheus Piza, Maja Somrak, Eric Vergo, Juehang Qin, Benjámín Borbás, Eric Chu, Jack Lindsey, Antoine Jallon, I. M. J. McInnis, Evan Chen, Avi Semler, Luk Gloor, Tej Shah, Marc Carauleanu, Pascal Lauer, Tran Duc Huy, Hossein Shahrtash, Emilien Duc, Lukas Lewark, Assaf Brown, Samuel Albanie, Brian Weber, Warren S. Vaz, Pierre Clavier, Yiyang Fan, Gabriel Poesia Reis e Silva, Long, Lian, Marcus Abramovitch, Xi Jiang, Sandra Mendoza, Murat Islam, Juan Gonzalez, Vasiliios Mavroudis, Justin Xu, Pawan Kumar, Laxman Prasad Goswami, Daniel Bugas, Nasser Heydari, Ferenc Jeanplong, Thorben Jansen, Antonella Pinto, Archimedes Apronti, Abdallah Galal, Ng Ze-An, Ankit Singh, Tong Jiang, Joan of Arc Xavier, Kanu Priya Agarwal, Mohammed Berkani, Gang Zhang, Zhehang Du, Benedito Alves de Oliveira Junior, Dmitry Malishev, Nicolas Remy, Taylor D. Hartman, Tim Tarver,

Stephen Mensah, Gautier Abou Loume, Wiktor Morak, Farzad Habibi, Sarah Hoback, Will Cai, Javier Gimenez, Roselynn Grace Montecillo, Jakub Lucki, Russell Campbell, Asankhaya Sharma, Khalida Meer, Shreen Gul, Daniel Espinosa Gonzalez, Xavier Alapont, Alex Hoover, Gunjan Chhablani, Freddie Vargus, Arunim Agarwal, Yibo Jiang, Deepakkumar Patil, David Outevsky, Kevin Joseph Scaria, Rajat Maheshwari, Abdelkader Dendane, Priti Shukla, Ashley Cartwright, Sergei Bogdanov, Niels Mündler, Sören Möller, Luca Arnaboldi, Kunvar Thaman, Muhammad Rehan Siddiqi, Prajvi Saxena, Himanshu Gupta, Tony Fruhauff, Glen Sherman, Mátyás Vincze, Siranut Usawasutsakorn, Dylan Ler, Anil Radhakrishnan, Innocent Enyekwe, Sk Md Salauddin, Jiang Muzhen, Aleksandr Maksapetyan, Vivien Rossbach, Chris Harjadi, Mohsen Bahaloohoreh, Claire Sparrow, Jasdeep Sidhu, Sam Ali, Song Bian, John Lai, Eric Singer, Justine Leon Uro, Greg Bateman, Mohamed Sayed, Ahmed Menshawy, Darling Duclosel, Dario Bezzi, Yashaswini Jain, Ashley Aaron, Murat Tiryakioglu, Sheeshram Siddh, Keith Krenek, Imad Ali Shah, Jun Jin, Scott Creighton, Denis Peskoff, Zienab EL-Wasif, Ragavendran P V, Michael Richmond, Joseph McGowan, Tejal Patwardhan, Hao-Yu Sun, Ting Sun, Nikola Zubić, Samuele Sala, Stephen Ebert, Jean Kaddour, Manuel Schottdorf, Dianzhuo Wang, Gerol Petruzella, Alex Meiburg, Tilen Medved, Ali ElSheikh, S Ashwin Hebbar, Lorenzo Vaquero, Xianjun Yang, Jason Poulos, Vilém Zouhar, Sergey Bogdanik, Mingfang Zhang, Jorge Sanz-Ros, David Anugraha, Yinwei Dai, Anh N. Nhu, Xue Wang, Ali Anil Demircali, Zhibai Jia, Yuyin Zhou, Juncheng Wu, Mike He, Nitin Chandok, Aarush Sinha, Gaoxiang Luo, Long Le, Mickaël Noyé, Michał Perelkiewicz, Ioannis Pantidis, Tianbo Qi, Soham Sachin Purohit, Letitia Parcalabescu, Thai-Hoa Nguyen, Genta Indra Winata, Edoardo M. Ponti, Hanchen Li, Kaustubh Dhole, Jongee Park, Dario Abbondanza, Yuanli Wang, Anupam Nayak, Diogo M. Caetano, Antonio A. W. L. Wong, Maria del Rio-Chanona, Dániel Kondor, Pieter Francois, Ed Chaltrey, Jakob Zsombok, Dan Hoyer, Jenny Reddish, Jakob Hauser, Francisco-Javier Rodrigo-Ginés, Suchandra Datta, Maxwell Shepherd, Thom Kamphuis, Qizheng Zhang, Hyunjun Kim, Ruiji Sun, Jianzhu Yao, Franck Dernoncourt, Satyapriya Krishna, Sina Rismanchian, Bonan Pu, Francesco Pinto, Yingheng Wang, Kumar Shridhar, Kalon J. Overholt, Glib Briia, Hieu Nguyen, David, Soler Bartomeu, Tony CY Pang, Adam Wecker, Yifan Xiong, Fanfei Li, Lukas S. Huber, Joshua Jaeger, Romano De Maddalena, Xing Han Lù, Yuhui Zhang, Claas Beger, Patrick Tser Jern Kon, Sean Li, Vivek Sanker, Ming Yin, Yihao Liang, Xinlu Zhang, Ankit Agrawal, Li S. Yifei, Zechen Zhang, Mu Cai, Yasin Sonmez, Costin Cozianu, Changhao Li, Alex Slen, Shoubin Yu, Hyun Kyu Park, Gabriele Sarti, Marcin Briański, Alessandro Stolfo, Truong An Nguyen, Mike Zhang, Yotam Perlit, Jose Hernandez-Orallo, Runjia Li, Amin Shabani, Felix Juefei-Xu, Shikhar Dhingra, Orr Zohar, My Chiffon Nguyen, Alexander Pondaven, Abdurrahim Yilmaz, Xuandong Zhao, Chuanyang Jin, Muyan Jiang, Stefan Todoran, Xinyao Han, Jules Kreuer, Brian Rabern, Anna Plassart, Martino Maggetti, Luther Yap, Robert Geirhos, Jonathon Kean, Dingsu Wang, Sina Mollaei, Chenkai Sun, Yifan Yin, Shiqi Wang, Rui Li, Yaowen Chang, Anjiang Wei, Alice Bizeul, Xiaohan Wang, Alexandre Oliveira Arrais, Kushin Mukherjee, Jorge Chamorro-Padial, Jiachen Liu, Xingyu Qu, Junyi Guan, Adam Bouyamourn, Shuyu Wu, Martyna Plomecka, Junda Chen, Mengze Tang, Jiaqi Deng, Shreyas Subramanian, Haocheng Xi, Haoxuan Chen, Weizhi Zhang, Yinuo Ren, Haoqin Tu, Sejong Kim, Yushun Chen, Sara Vera Marjanović, Junwoo Ha, Grzegorz Luczyna, Jeff J. Ma, Zewen Shen, Dawn Song, Cedegao E. Zhang, Zhun Wang, Gaël Gendron, Yunze Xiao, Leo Smucker, Erica Weng, Kwok Hao Lee, Zhe Ye, Stefano Ermon, Ignacio D. Lopez-Miguel, Theo Knights, Anthony Gitter, Namkyu Park, Boyi Wei, Hongzheng Chen, Kunal Pai, Ahmed Elkhanany, Han Lin, Philipp D. Siedler, Jichao Fang, Ritwik Mishra, Károly Zsolnai-Fehér, Xilin Jiang, Shadab Khan, Jun Yuan, Rishab Kumar Jain, Xi Lin, Mike Peterson, Zhe Wang, Aditya Malusare, Maosen Tang, Isha Gupta, Ivan Fosin, Timothy Kang, Barbara Dworakowska, Kazuki Matsumoto, Guangyao Zheng, Gerben Sewuster, Jorge Pretel Villanueva, Ivan Rannev, Igor Chernyavsky, Jiale Chen, Deepayan Banik, Ben Racz, Wenchao Dong, Jianxin Wang, Laila Bashmal, Duarte V. Gonçalves, Wei Hu, Kaushik Bar, Ondrej Bohdal, Atharv Singh Patlan, Shehzaad Dhuliawala, Caroline Geirhos, Julien Wist, Yuval Kansal, Bingsen Chen, Kutay Tire, Atak Talay Yücel, Brandon Christof, Veerupaksh Singla, Zijian Song, Sanxing Chen, Jiaxin Ge, Kaustubh Ponske, Isaac Park, Tianneng Shi, Martin Q. Ma, Joshua Mak, Sherwin Lai, Antoine Moulin, Zhuo Cheng, Zhanda Zhu, Ziyi Zhang, Vaidehi Patil, Ketan Jha, Qitong Men, Jiakuan Wu, Tianchi Zhang, Bruno Hebling Vieira, Alham Fikri Aji, Jae-Won Chung, Mohammed Mahfoud, Ha Thi Hoang, Marc Sperzel, Wei Hao, Kristof Meding, Sihan Xu, Vassilis Kostakos, Davide Manini, Yueying Liu, Christopher Toukmaji, Jay Paek, Eunmi Yu, Arif Engin Demircali, Zhiyi Sun, Ivan Dewerpe, Hongsen Qin, Roman Pflugfelder, James Bailey, Johnathan Morris, Ville Heilala, Sybille Rosset, Zishun Yu, Peter E. Chen, Woongyeong Yeo, Eeshaan Jain, Ryan Yang, Sreekar Chigurupati, Julia Chernyavsky, Sai Prajwal Reddy, Subhashini Venugopalan, Hunar Batra, Core Francisco Park, Hieu Tran, Guilherme Maximiano, Genghan Zhang, Yizhuo Liang, Hu Shiyu, Rongwu Xu, Rui Pan, Siddharth Suresh, Ziqi Liu, Samaksh Gulati, Songyang Zhang, Peter Turchin, Christopher W. Bartlett, Christopher R. Scotese, Phuong M. Cao, Ben Wu, Jacek Karwowski, Davide Scaramuzza, Aakaash Nattanmai, Gordon McKellips, Anish Cheraku, Asim Suhail, Ethan Luo, Marvin Deng, Jason Luo, Ashley Zhang, Kavin Jindel, Jay Paek, Kasper Halevy, Allen Baranov, Michael Liu, Advait Avadhanam, David Zhang, Vincent Cheng, Brad Ma, Evan Fu, Liam Do, Joshua Lass, Hubert Yang, Surya Sunkari, Vishruth Bharath, Violet Ai, James Leung, Rishit Agrawal, Alan Zhou, Kevin Chen, Tejas Kalpathi, Ziqi Xu, Gavin Wang, Tyler Xiao, Erik Maung, Sam Lee, Ryan

- Yang, Roy Yue, Ben Zhao, Julia Yoon, Sunny Sun, Aryan Singh, Ethan Luo, Clark Peng, Tyler Osbey, Taozhi Wang, Daryl Echeazu, Hubert Yang, Timothy Wu, Spandan Patel, Vidhi Kulkarni, Vijaykaarti Sundarapandiyam, Ashley Zhang, Andrew Le, Zafir Nasim, Srikar Yalam, Ritesh Kasamsetty, Soham Samal, Hubert Yang, David Sun, Nihar Shah, Abhijeet Saha, Alex Zhang, Leon Nguyen, Laasya Nagumalli, Kaixin Wang, Alan Zhou, Aidan Wu, Jason Luo, Anwith Telluri, Summer Yue, Alexandr Wang, and Dan Hendrycks. Humanity’s last exam, 2025.
- [27] Naman Jain, King Han, Alex Gu, Wen-Ding Li, Fanjia Yan, Tianjun Zhang, Sida Wang, Armando Solar-Lezama, Koushik Sen, and Ion Stoica. LiveCodeBench: Holistic and Contamination Free Evaluation of Large Language Models for Code. *arXiv preprint*, 2024.
- [28] Neel Guha, Julian Nyarko, Daniel E. Ho, Christopher Ré, Adam Chilton, Aditya Narayana, Alex Chohlas-Wood, Austin Peters, Brandon Waldon, Daniel N. Rockmore, Diego Zambrano, Dmitry Talisman, Enam Hoque, Faiz Surani, Frank Fagan, Galit Sarfaty, Gregory M. Dickinson, Haggai Porat, Jason Hegland, Jessica Wu, Joe Nudell, Joel Niklaus, John Nay, Jonathan H. Choi, Kevin Tobia, Margaret Hagan, Megan Ma, Michael Livermore, Nikon Rasumov-Rahe, Nils Holzenberger, Noam Kolt, Peter Henderson, Sean Rehaag, Sharad Goel, Shang Gao, Spencer Williams, Sunny Gandhi, Tom Zur, Varun Iyer, and Zehua Li. Legalbench: A collaboratively built benchmark for measuring legal reasoning in large language models, 2023.
- [29] Carlos E Jimenez, John Yang, Alexander Wettig, Shunyu Yao, Kexin Pei, Ofir Press, and Karthik R Narasimhan. SWE-bench: Can language models resolve real-world github issues? In *The Twelfth International Conference on Learning Representations*, 2024.
- [30] Yilun Zhao, Hongjun Liu, Yitao Long, Rui Zhang, Chen Zhao, and Arman Cohan. Financemath: Knowledge-intensive math reasoning in finance domains, 2024.

A Experiments Result with Further Analysis

A.1 Full Table of all metrics

Table 7 shows all metrics of 5 models on 9 dataset (7 domains), with this projected to Domain Expertise, the min/max value is set as bold in Table 8.

Table 7: Comparison of Qwen3, DeepSeek-R1-0528, and GLM-4.6 benchmarks.

Model	Partition	Domain	S_{spec}	R_{eff}	S_{iso}	$R_{\text{RSS}}(G_{\theta^*})$	$R_{\text{RSS}}(G_{\theta^*})$	$R_{\text{RSS}}(G_{\theta^*})$	$E_{\text{NGR}}^{(n)}$	$E_{\text{NGR}}^{(n)}$	$E_{\text{NGR}}^{(n)}$	$E_{\text{NGR}}^{(n)}$	$G_{\text{G-NGR}}^{(n)}$	$G_{\text{G-NGR}}^{(n)}$	$G_{\text{G-NGR}}^{(n)}$	$G_{\text{G-NGR}}^{(n)}$
Qwen3-30B-Instruct	aime 2025	Math	0.63	0.44	0.56	3.71E-05	1.70E-05	1.07E-05	17.23%	1.05%	0.12%	0.01%	19.78%	4.37%	0.69%	0.04%
	AllenAI SciQ (Val)	Science	0.80	0.45	0.54	3.76E-05	2.15E-05	8.83E-06	27.47%	5.70%	1.46%	0.24%	29.00%	11.01%	3.78%	0.81%
	BigBio MedQA (Dev)	Medical	0.90	0.50	0.57	3.74E-05	1.97E-05	9.63E-06	31.98%	6.94%	1.67%	0.23%	37.76%	16.87%	6.39%	1.52%
	BigBio MedQA (Test)	Medical2	0.91	0.50	0.57	2.93E-05	1.86E-05	1.00E-05	32.01%	6.95%	1.67%	0.22%	37.83%	17.04%	6.62%	1.66%
	CAIS HLE	Knowledge	0.43	0.37	0.44	4.77E-05	2.38E-05	1.16E-05	22.01%	2.57%	0.57%	0.17%	14.40%	3.59%	0.80%	0.12%
	LiveCodeBench (Test)	Code	0.44	0.39	0.54	4.49E-05	2.09E-05	9.79E-06	22.69%	3.79%	1.01%	0.23%	20.99%	7.60%	2.85%	0.83%
	Nguha LegalBench	Legal	0.95	0.47	0.64	4.14E-05	1.85E-05	8.75E-06	25.69%	5.31%	1.50%	0.31%	30.67%	11.92%	4.09%	0.86%
	Princeton SWE-bench (Test)	Code2	0.63	0.44	0.62	3.74E-05	2.04E-05	1.05E-05	22.05%	2.05%	0.26%	0.03%	19.79%	5.27%	1.13%	0.13%
	Yale-FinanceMath (Val)	Finance	0.57	0.41	0.58	4.60E-05	1.98E-05	1.05E-05	24.89%	3.40%	0.60%	0.08%	29.10%	10.46%	2.98%	0.53%
	Avg.			0.70	0.44	0.56	3.99E-05	2.00E-05	1.00E-05	25.11%	4.20%	0.98%	0.17%	26.59%	9.79%	3.26%
Qwen3-30B-Thinking	AIME 2025	Math	0.67	0.44	0.55	3.82E-05	1.92E-05	1.04E-05	17.18%	1.31%	0.15%	0.01%	20.02%	5.14%	1.00%	0.09%
	AllenAI SciQ (Val)	Science	0.79	0.45	0.43	4.09E-05	1.70E-05	9.54E-06	21.00%	2.13%	0.28%	0.02%	19.66%	4.63%	0.87%	0.09%
	BigBio MedQA (Dev)	Medical	1.09	0.54	0.58	3.14E-05	1.41E-05	9.13E-06	27.82%	4.70%	0.97%	0.12%	37.28%	15.05%	5.59%	1.73%
	BigBio MedQA (Test)	Medical2	1.09	0.54	0.58	3.15E-05	1.76E-05	8.80E-06	27.84%	4.72%	0.99%	0.13%	37.23%	15.07%	5.65%	1.76%
	CAIS HLE	Knowledge	0.47	0.39	0.38	4.36E-05	2.07E-05	1.04E-05	20.17%	2.13%	0.36%	0.06%	13.59%	2.74%	0.52%	0.06%
	LiveCodeBench (Test)	Code	0.64	0.46	0.41	4.80E-05	2.06E-05	1.17E-05	19.13%	1.99%	0.34%	0.04%	19.77%	4.92%	1.16%	0.18%
	Nguha LegalBench	Legal	0.98	0.48	0.53	3.45E-05	1.79E-05	7.26E-06	22.10%	2.69%	0.45%	0.04%	24.96%	7.55%	1.93%	0.27%
	Princeton SWE-bench (Test)	Code2	0.76	0.46	0.55	3.48E-05	2.04E-05	1.09E-05	20.24%	1.57%	0.19%	0.03%	23.85%	6.51%	1.42%	0.17%
	Yale-FinanceMath (Val)	Finance	0.62	0.42	0.52	4.33E-05	2.15E-05	9.19E-06	22.22%	2.66%	0.43%	0.04%	24.32%	6.96%	1.52%	0.17%
	Avg.			0.79	0.46	0.50	3.85E-05	1.88E-05	9.70E-06	21.97%	2.65%	0.46%	0.05%	24.52%	7.62%	2.18%
Qwen3-235B-Thinking	AIME 2025	Math	0.74	0.28	0.51	3.96E-05	1.87E-05	9.34E-06	19.26%	1.73%	0.25%	0.04%	21.20%	5.34%	1.13%	0.16%
	AllenAI SciQ (Val)	Science	0.70	0.26	0.45	4.34E-05	1.84E-05	9.65E-06	22.68%	2.76%	0.48%	0.05%	17.91%	4.34%	0.89%	0.10%
	BigBio MedQA (Dev)	Medical	0.99	0.31	0.58	3.74E-05	1.99E-05	8.60E-06	28.50%	4.87%	1.10%	0.17%	36.77%	15.15%	5.50%	1.39%
	BigBio MedQA (Test)	Medical2	0.99	0.31	0.58	3.56E-05	1.75E-05	8.54E-06	28.51%	4.87%	1.11%	0.17%	36.71%	15.10%	5.47%	1.39%
	CAIS HLE	Knowledge	0.49	0.24	0.37	4.85E-05	2.39E-05	1.28E-05	21.88%	2.61%	0.50%	0.08%	13.10%	2.63%	0.51%	0.08%
	LiveCodeBench (Test)	Code	0.64	0.28	0.44	3.89E-05	1.92E-05	9.38E-06	21.59%	2.62%	0.48%	0.07%	21.11%	5.82%	1.50%	0.26%
	Nguha LegalBench	Legal	0.94	0.27	0.56	3.43E-05	1.97E-05	9.05E-06	24.50%	3.32%	0.60%	0.07%	27.04%	8.28%	1.90%	0.21%
	Princeton SWE-bench (Test)	Code2	0.76	0.27	0.57	3.89E-05	1.90E-05	9.62E-06	21.41%	1.71%	0.19%	0.02%	20.57%	4.92%	0.86%	0.08%
	Yale-FinanceMath (Val)	Finance	0.57	0.26	0.51	4.13E-05	1.93E-05	1.01E-05	24.53%	3.58%	0.68%	0.09%	26.29%	8.46%	2.27%	0.39%
	Avg.			0.76	0.28	0.51	3.98E-05	1.95E-05	9.68E-06	23.65%	3.12%	0.60%	0.08%	24.52%	7.78%	2.23%
DeepSeek-R1-0528	AIME 2025	Math	0.24	0.49	0.36	3.32E-05	1.71E-05	8.22E-06	18.69%	1.87%	0.30%	0.04%	13.93%	3.12%	0.63%	0.08%
	AllenAI SciQ (Val)	Science	0.24	0.47	0.31	3.45E-05	1.75E-05	8.54E-06	21.23%	2.88%	0.64%	0.09%	10.67%	2.60%	0.66%	0.11%
	BigBio MedQA (Dev)	Medical	0.31	0.54	0.31	3.42E-05	1.68E-05	8.34E-06	19.43%	2.45%	0.48%	0.06%	13.08%	3.18%	0.78%	0.11%
	BigBio MedQA (Test)	Medical2	0.31	0.54	0.31	3.35E-05	1.70E-05	8.29E-06	19.37%	2.41%	0.47%	0.06%	13.02%	3.11%	0.75%	0.11%
	CAIS HLE	Knowledge	0.10	0.28	0.22	3.70E-05	1.92E-05	8.96E-06	18.60%	1.95%	0.37%	0.06%	5.87%	1.00%	0.21%	0.03%
	LiveCodeBench (Test)	Code	0.21	0.46	0.36	3.56E-05	1.77E-05	8.56E-06	21.72%	2.85%	0.60%	0.10%	12.26%	3.36%	0.93%	0.20%
	Nguha LegalBench	Legal	0.31	0.56	0.39	3.40E-05	1.76E-05	8.21E-06	20.51%	2.36%	0.40%	0.04%	14.24%	3.73%	0.83%	0.10%
	Princeton SWE-bench (Test)	Code2	0.23	0.49	0.40	3.35E-05	1.69E-05	8.15E-06	22.07%	2.62%	0.48%	0.06%	14.81%	3.90%	0.89%	0.12%
	Yale-FinanceMath (Val)	Finance	0.22	0.47	0.33	3.49E-05	1.71E-05	8.32E-06	18.82%	2.00%	0.39%	0.07%	13.28%	3.21%	0.75%	0.13%
	Avg.			0.24	0.48	0.33	3.45E-05	1.74E-05	8.40E-06	20.05%	2.38%	0.46%	0.06%	12.35%	3.02%	0.71%
DeepSeek-R1-0528	aime 2025	Math	0.35	0.49	0.42	3.97E-05	2.03E-05	1.07E-05	19.80%	1.76%	0.23%	0.02%	17.52%	4.00%	0.83%	0.11%
	AllenAI SciQ (Val)	Science	0.33	0.47	0.31	4.24E-05	2.20E-05	1.10E-05	25.35%	3.72%	0.77%	0.10%	13.92%	3.60%	0.83%	0.12%
	BigBio MedQA (Dev)	Medical	0.47	0.59	0.39	3.98E-05	2.03E-05	9.98E-06	28.39%	5.43%	1.44%	0.27%	23.92%	8.97%	3.16%	0.76%
	BigBio MedQA (Test)	Medical2	0.47	0.59	0.39	4.18E-05	2.11E-05	1.01E-05	28.35%	5.41%	1.43%	0.26%	23.72%	8.83%	3.08%	0.73%
	CAIS HLE	Knowledge	0.15	0.30	0.26	4.49E-05	2.37E-05	1.13E-05	24.20%	3.61%	0.83%	0.15%	10.99%	2.94%	0.84%	0.18%
	LiveCodeBench (Test)	Code	0.30	0.46	0.34	4.22E-05	2.26E-05	1.13E-05	22.40%	2.69%	0.44%	0.04%	12.64%	2.92%	0.56%	0.05%
	Nguha LegalBench	Legal	0.41	0.54	0.38	4.31E-05	2.01E-05	9.72E-06	24.59%	3.34%	0.64%	0.08%	18.72%	5.57%	1.43%	0.24%
	Princeton SWE-bench (Test)	Code2	0.23	0.42	0.39	4.50E-05	2.25E-05	1.11E-05	21.47%	1.91%	0.28%	0.03%	13.17%	2.85%	0.54%	0.06%
	Yale-FinanceMath (Val)	Finance	0.33	0.51	0.37	4.26E-05	2.23E-05	1.02E-05	24.11%	3.08%	0.50%	0.05%	18.73%	5.35%	1.23%	0.15%
	Avg.			0.34	0.49	0.36	4.24E-05	2.16E-05	1.06E-05	24.29%	3.44%	0.73%	0.11%	17.04%	5.00%	1.39%

Table 8 show that these suite of metrics serve as a comprehensive estimation of expertise which focus on different aspects of expertise, token level (S_{spec} , R_{eff} , S_{iso}), complexity metric ($R_{\text{RSS}}(G_{\theta^*})$ -500, $R_{\text{RSS}}(G_{\theta^*})$ -1000, $R_{\text{RSS}}(G_{\theta^*})$ -2000) and sequence level ($E_{\text{NGR}}^{(n)}$ -2, $E_{\text{NGR}}^{(n)}$ -5, $E_{\text{NGR}}^{(n)}$ -10, $E_{\text{NGR}}^{(n)}$ -20, $G_{\text{G-NGR}}^{(n)}$ -2, $G_{\text{G-NGR}}^{(n)}$ -5, $G_{\text{G-NGR}}^{(n)}$ -10, $G_{\text{G-NGR}}^{(n)}$ -20).

Table 8: Expertise Results: Grouped by Partition

Partition	Model	Domain	S _{spec}	R _{eff}	S _{iso}	R _{RSS-500}	R _{RSS-1000}	R _{RSS-2000}	E _{NGR-2} ⁽ⁿ⁾	E _{NGR-5} ⁽ⁿ⁾	E _{NGR-10} ⁽ⁿ⁾	E _{NGR-20} ⁽ⁿ⁾	G _{G-NGR-2} ⁽ⁿ⁾	G _{G-NGR-5} ⁽ⁿ⁾	G _{G-NGR-10} ⁽ⁿ⁾	G _{G-NGR-20} ⁽ⁿ⁾
AllenAI SciQ (Val)	DeepSeek-R1-0528	Science	0.24	0.47	0.31	3.45E-05	1.75E-05	8.54E-06	21.23%	2.88%	0.64%	0.09%	10.67%	2.60%	0.66%	0.11%
	DeepSeek-R1-0528		0.33	0.47	0.31	4.24E-05	2.20E-05	1.10E-05	25.35%	3.72%	0.77%	0.10%	13.92%	3.60%	0.83%	0.12%
	Qwen3-235B-Thinking		0.70	0.26	0.45	4.34E-05	1.84E-05	9.65E-06	22.68%	2.76%	0.48%	0.05%	17.91%	4.34%	0.89%	0.10%
	Qwen3-30B-Instruct		0.80	0.45	0.54	3.76E-05	2.15E-05	8.83E-06	27.47%	5.70%	1.46%	0.24%	29.00%	11.01%	3.78%	0.81%
	Qwen3-30B-Thinking		0.79	0.45	0.43	4.09E-05	1.70E-05	9.54E-06	21.00%	2.13%	0.28%	0.02%	19.66%	4.63%	0.87%	0.09%
BigBio MedQA (Dev)	DeepSeek-R1-0528	Medical	0.31	0.54	0.31	3.42E-05	1.68E-05	8.34E-06	19.43%	2.45%	0.48%	0.06%	13.08%	3.18%	0.78%	0.11%
	DeepSeek-R1-0528		0.47	0.59	0.39	3.98E-05	2.03E-05	9.98E-06	28.39%	5.43%	1.44%	0.27%	23.92%	8.97%	3.16%	0.76%
	Qwen3-235B-Thinking		0.99	0.31	0.58	3.74E-05	1.99E-05	8.60E-06	28.50%	4.87%	1.10%	0.17%	36.77%	15.15%	5.50%	1.39%
	Qwen3-30B-Instruct		0.90	0.50	0.57	2.93E-05	1.97E-05	9.63E-06	31.98%	6.94%	1.67%	0.23%	37.76%	16.87%	6.39%	1.52%
	Qwen3-30B-Thinking		1.09	0.54	0.58	3.14E-05	1.41E-05	9.13E-06	27.82%	4.70%	0.97%	0.12%	37.28%	15.05%	5.59%	1.73%
BigBio MedQA (Test)	DeepSeek-R1-0528	Medical2	0.31	0.54	0.31	3.35E-05	1.70E-05	8.29E-06	19.37%	2.41%	0.47%	0.06%	13.02%	3.11%	0.75%	0.11%
	DeepSeek-R1-0528		0.47	0.59	0.39	4.18E-05	2.11E-05	1.01E-05	28.35%	5.41%	1.43%	0.26%	23.72%	8.83%	3.08%	0.73%
	Qwen3-235B-Thinking		0.99	0.31	0.58	3.56E-05	1.75E-05	8.54E-06	28.51%	4.87%	1.11%	0.17%	36.71%	15.10%	5.47%	1.39%
	Qwen3-30B-Instruct		0.91	0.50	0.57	2.93E-05	1.86E-05	1.00E-05	32.01%	6.95%	1.67%	0.22%	37.83%	17.04%	6.62%	1.66%
	Qwen3-30B-Thinking		1.09	0.54	0.58	3.15E-05	1.76E-05	8.80E-06	27.84%	4.72%	0.99%	0.13%	37.23%	15.07%	5.65%	1.76%
CAIS HLE	DeepSeek-R1-0528	Knowledge	0.10	0.28	0.22	3.70E-05	1.92E-05	8.96E-06	18.60%	1.95%	0.37%	0.06%	5.87%	1.00%	0.21%	0.03%
	DeepSeek-R1-0528		0.15	0.30	0.26	4.49E-05	2.37E-05	1.13E-05	24.20%	3.61%	0.83%	0.15%	10.99%	2.94%	0.84%	0.18%
	Qwen3-235B-Thinking		0.49	0.24	0.37	4.85E-05	2.39E-05	1.28E-05	21.88%	2.61%	0.50%	0.08%	13.10%	2.63%	0.51%	0.08%
	Qwen3-30B-Instruct		0.43	0.37	0.44	4.77E-05	2.38E-05	1.16E-05	22.01%	2.57%	0.57%	0.17%	14.40%	3.59%	0.80%	0.12%
	Qwen3-30B-Thinking		0.47	0.39	0.38	4.36E-05	2.07E-05	1.04E-05	20.17%	2.13%	0.36%	0.06%	13.59%	2.74%	0.52%	0.06%
LiveCodeBench (Test)	DeepSeek-R1-0528	Code	0.21	0.46	0.36	3.56E-05	1.77E-05	8.56E-06	21.72%	2.85%	0.60%	0.10%	12.26%	3.36%	0.93%	0.20%
	DeepSeek-R1-0528		0.30	0.46	0.34	4.22E-05	2.26E-05	1.13E-05	22.40%	2.69%	0.44%	0.04%	12.64%	2.92%	0.56%	0.05%
	Qwen3-235B-Thinking		0.64	0.28	0.44	3.89E-05	1.92E-05	9.38E-06	21.59%	2.62%	0.48%	0.07%	21.11%	5.82%	1.50%	0.26%
	Qwen3-30B-Instruct		0.44	0.39	0.54	4.49E-05	2.09E-05	9.79E-06	22.69%	3.79%	1.01%	0.23%	20.99%	7.60%	2.85%	0.83%
	Qwen3-30B-Thinking		0.64	0.46	0.41	4.80E-05	2.06E-05	1.17E-05	19.13%	1.99%	0.34%	0.04%	19.77%	4.92%	1.16%	0.18%
Nguha LegalBench	DeepSeek-R1-0528	Legal	0.31	0.56	0.39	3.40E-05	1.76E-05	8.21E-06	20.51%	2.36%	0.40%	0.04%	14.24%	3.73%	0.83%	0.10%
	DeepSeek-R1-0528		0.41	0.54	0.38	4.31E-05	2.01E-05	9.72E-06	24.59%	3.34%	0.64%	0.08%	18.72%	5.57%	1.43%	0.24%
	Qwen3-235B-Thinking		0.94	0.27	0.56	3.43E-05	1.97E-05	9.05E-06	24.50%	3.32%	0.60%	0.07%	27.04%	8.28%	1.90%	0.21%
	Qwen3-30B-Instruct		0.95	0.47	0.64	4.14E-05	1.85E-05	8.75E-06	25.69%	5.31%	1.50%	0.31%	30.67%	11.92%	4.09%	0.86%
	Qwen3-30B-Thinking		0.98	0.48	0.53	3.45E-05	1.79E-05	7.26E-06	22.10%	2.69%	0.45%	0.04%	24.96%	7.55%	1.93%	0.27%
Princeton SWE-bench (Test)	DeepSeek-R1-0528	Code2	0.23	0.49	0.40	3.35E-05	1.69E-05	8.15E-06	22.07%	2.62%	0.48%	0.06%	14.81%	3.90%	0.89%	0.12%
	DeepSeek-R1-0528		0.23	0.42	0.39	4.50E-05	2.25E-05	1.11E-05	21.47%	1.91%	0.28%	0.03%	13.17%	2.85%	0.54%	0.06%
	Qwen3-235B-Thinking		0.76	0.27	0.57	3.89E-05	1.90E-05	9.62E-06	21.41%	1.71%	0.19%	0.02%	20.57%	4.92%	0.86%	0.08%
	Qwen3-30B-Instruct		0.63	0.44	0.62	3.74E-05	2.04E-05	1.05E-05	22.05%	2.05%	0.26%	0.03%	19.79%	5.27%	1.13%	0.13%
	Qwen3-30B-Thinking		0.76	0.46	0.55	3.48E-05	2.04E-05	1.09E-05	20.24%	1.57%	0.19%	0.03%	23.85%	6.51%	1.42%	0.17%
Yale-FinanceMath (Val)	DeepSeek-R1-0528	Finance	0.22	0.47	0.33	3.49E-05	1.71E-05	8.32E-06	18.82%	2.00%	0.39%	0.07%	13.28%	3.21%	0.75%	0.13%
	DeepSeek-R1-0528		0.33	0.51	0.37	4.26E-05	2.23E-05	1.02E-05	24.11%	3.08%	0.50%	0.05%	18.73%	5.35%	1.23%	0.15%
	Qwen3-235B-Thinking		0.57	0.26	0.51	4.13E-05	1.93E-05	1.01E-05	24.53%	3.58%	0.68%	0.09%	26.29%	8.46%	2.27%	0.39%
	Qwen3-30B-Instruct		0.57	0.41	0.58	4.60E-05	1.98E-05	1.05E-05	24.89%	3.40%	0.60%	0.08%	29.10%	10.46%	2.98%	0.53%
	Qwen3-30B-Thinking		0.62	0.42	0.52	4.33E-05	2.15E-05	9.19E-06	22.22%	2.66%	0.43%	0.04%	24.32%	6.96%	1.52%	0.17%
AIME 2025	DeepSeek-R1-0528	Math	0.24	0.49	0.36	3.32E-05	1.71E-05	8.22E-06	18.69%	1.87%	0.30%	0.04%	13.93%	3.12%	0.63%	0.08%
	DeepSeek-R1-0528		0.35	0.49	0.42	3.97E-05	2.03E-05	1.07E-05	19.80%	1.76%	0.23%	0.02%	17.52%	4.00%	0.83%	0.11%
	Qwen3-235B-Thinking		0.74	0.28	0.51	3.96E-05	1.87E-05	9.34E-06	19.26%	1.73%	0.25%	0.04%	21.20%	5.34%	1.13%	0.16%
	Qwen3-30B-Instruct		0.63	0.44	0.56	3.71E-05	1.70E-05	1.07E-05	17.23%	1.05%	0.12%	0.01%	19.78%	4.37%	0.69%	0.04%
	Qwen3-30B-Thinking		0.67	0.44	0.55	3.82E-05	1.92E-05	1.04E-05	17.18%	1.31%	0.15%	0.01%	20.02%	5.14%	1.00%	0.09%

A.2 Specialty Radar Map of all metrics

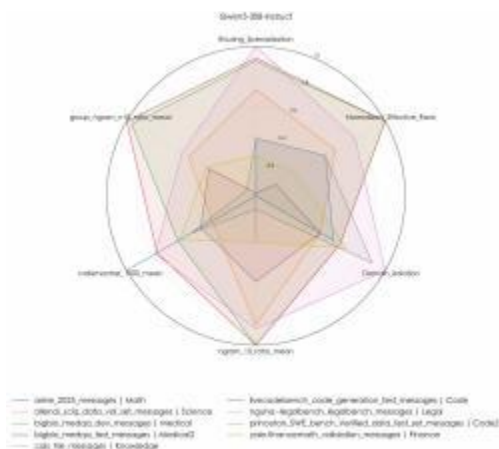
Model-Centric Specialization Profiles. Figures 6 and 7 illustrate the functional specialization landscape across diverse architectures and domains. These radar maps provide a model-centric architectural fingerprint, serving as a qualitative counterpart to the quantitative aggregations in our previous tables. This diagnostic framework enables a comparative appraisal of expertise even in the absence of explicit pre-training data access. By mapping these specialized "tributaries," we can identify the most promising foundation models for targeted post-training interventions, ensuring that the selected base architecture possesses the requisite structural priors for specific downstream expertise.

Figures 6 and 7 illustrate the domain-specific specialty profiles of the evaluated models. We observe that DeepSeek-R1-0528 exhibits a remarkably balanced distribution across all evaluated domains, suggesting a versatile routing strategy that avoids over-specialization in any single niche. In contrast, GLM 4.6 demonstrates a pronounced functional alignment with the Medical domain, where its specialization metrics significantly outperform its own baseline in other areas.

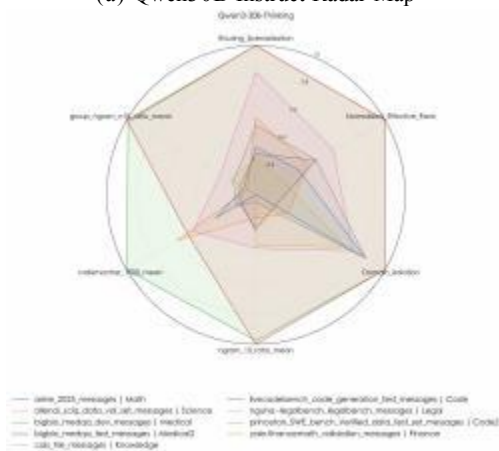
The aggregate comparison in Figure 8 highlights a clear hierarchy in routing paradigms:

- Qwen3-MoE consistently occupies the outermost boundary of the radar map, representing the peak of structural specialization and isolation among the tested series.
- GLM 4.6 follows as the second most specialized, maintaining strong modularity while allowing for more synergy than Qwen.
- Conversely, DeepSeek-R1 displays the lowest magnitude across specialization-specific metrics.

This reinforces our earlier observation that DeepSeek prioritizes a generalized, high-entropy routing manifold over rigid domain boundaries, favoring synergetic expert coordination to handle diverse reasoning tasks.



(a) Qwen30B Instruct Radar Map



(b) Qwen30B Thinking Radar Map

Figure 7: Domain-specific specialty fingerprints across LLM architectures(continue). The radar charts visualize relative expertise across diverse functional manifolds. Unlike static metric tables, these profiles reveal the structural orientation of each model, allowing for an informed selection of foundation models for domain-specific post-training specialization, regardless of the availability of original pre-training corpora

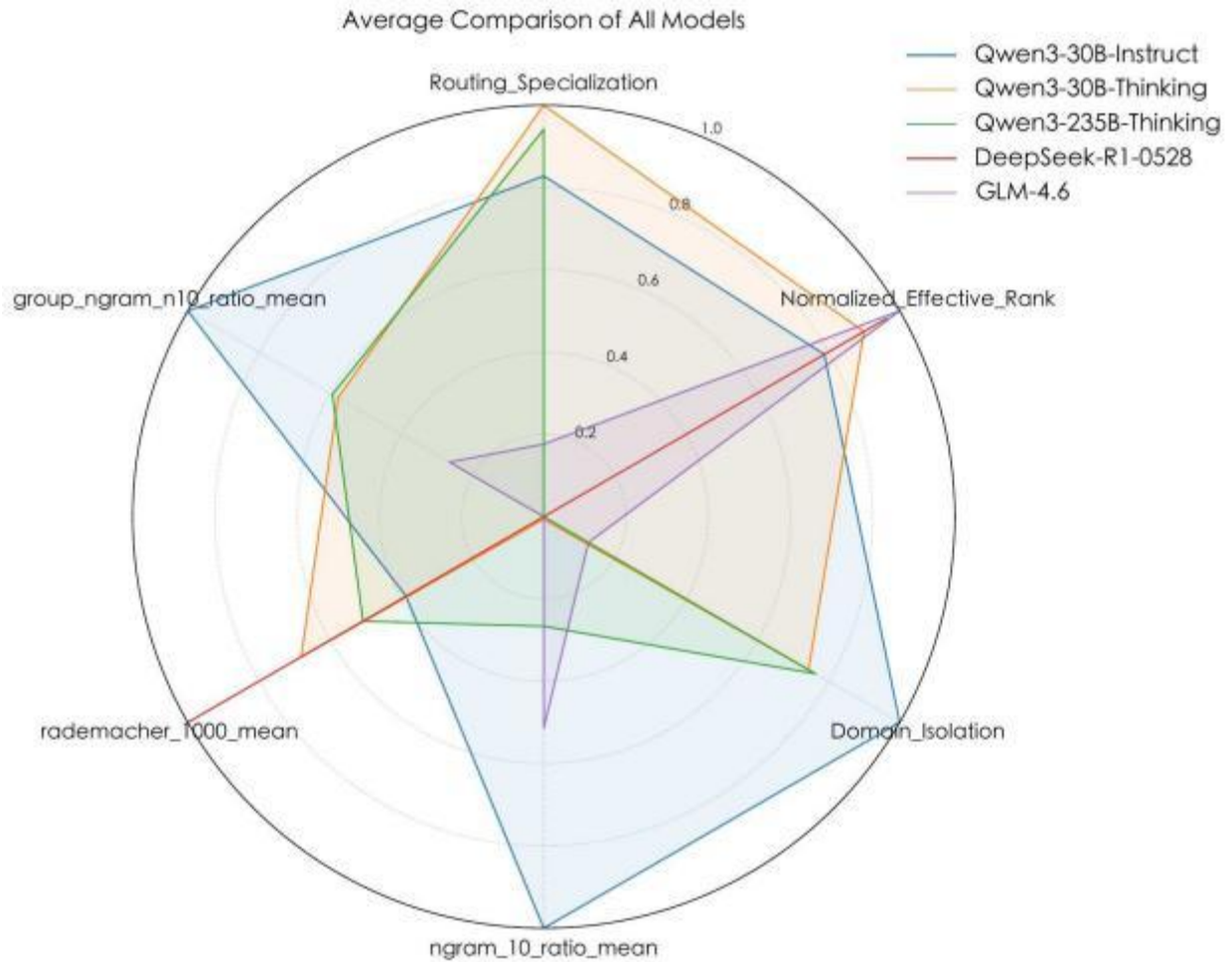


Figure 8: Comparative analysis of expert specialization and routing paradigms. a) Assessment of eleven metrics categorized into Specialization, Synergy, and Isolation across diverse domains. b) Contrast in routing behavior: DeepSeek-R1 exhibits lower Rademacher complexity, indicating high structural determinism; conversely, Qwen3-30B demonstrates superior N-gram expertise (temporal consistency), suggesting that its performance is critically dependent on sustained expert trajectories. c) Identification of two distinct paradigms: the Modular approach (Qwen: high specialization and isolation) with clear knowledge boundaries, and the Synergetic approach (DeepSeek/GLM: high effective rank) characterized by dynamic expert coordination.

A.3 Activation Map of different Models in different domain

In Section 4, we show partial results, the full results is as Qwen3-30B-A3B-Thinking(Figure 9), Qwen3-30B-A3B-Instruct(Figure 10), Qwen3-235B-A22B-Thinking(Figure 11), GLM 4.6(Figure 12) and DeepSeek-R1-0528(Figure 13) While Section 4 highlights selected representative cases, the full suite of expert activation landscapes—comprising Qwen3-30B-A3B-Thinking (Figures 9) and Qwen3-30B-A3B-Instruct (Figure 10), Qwen3-235B-A22B (Figure 11), GLM 4.6 (Figure 12), and DeepSeek-R1-0528 (Figure 13)—is provided for a granular cross-model comparison.

These empirical results exhibit high internal consistency with our global radar map assessment. We observe distinct domain-specific activation signatures across all evaluated architectures, though the topology of these signatures varies significantly:

- The Qwen Series: Shows highly concentrated activation "hotspots" that are strictly partitioned by domain, reinforcing its status as a Modular routing paradigm.
- GLM & DeepSeek: Display more diffused yet structured activation patterns. As shown in the heatmaps, these models exhibit a synergetic distribution, where a core set of shared experts is dynamically augmented by domain-specialized expert clusters.

The clear divergence in expert-usage statistics between "Instruct" and "Thinking" versions of the same model (e.g., Figures 9 vs. 10) further validates our Sequence-Aware Bellman Rank hypothesis, indicating that increased reasoning depth (CoT) fundamentally reconfigures the routing manifold to favor more persistent, long-range expert trajectories.

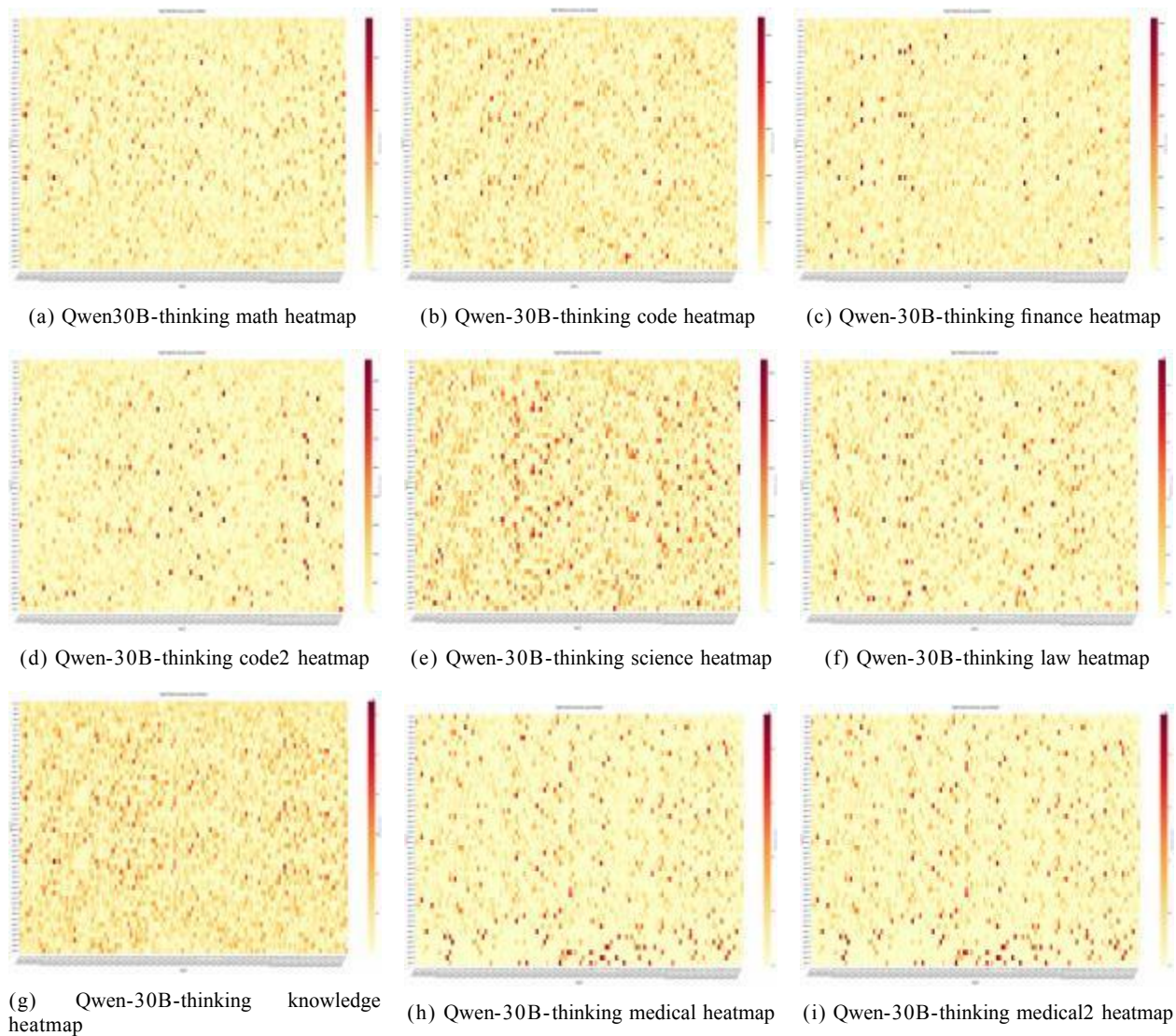


Figure 9: Qwen3-30B-A3B-Thinking model activation. a) Heterogeneous Expert Concentration: The model exhibits domain-specific activation densities; scientific domains are characterized by dense, clustered expert usage, whereas code and math domains demonstrate comparative sparsity in expert selection. b) Intradomain Variability: Significant fluctuations in activation intensity are observed even within the same domain; for example, different coding tasks trigger distinct expert sub-manifolds, reflecting the model’s granular adaptability to diverse problem complexities.

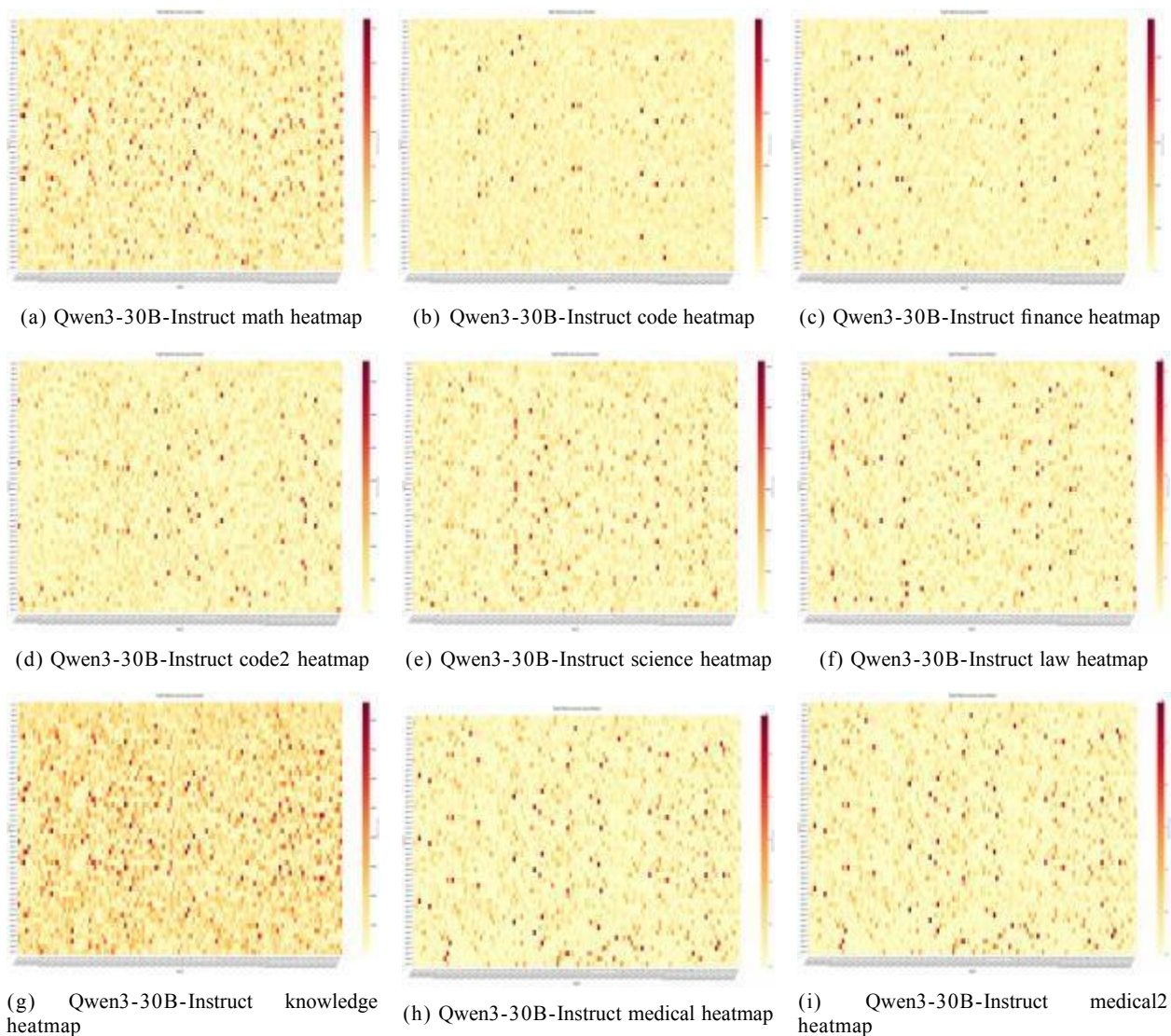


Figure 10: Qwen3-30B-A3B-Instruct model activation. a) Activation Gradients: Intensive expert recruitment is concentrated in knowledge and math domains, with pronounced sparsity elsewhere. b) Intra-domain Variance: Comparison between Code and Code2 reveals a shift in expert preference, suggesting that task-specific logic (e.g., script vs. algorithmic) triggers different expert sub-manifolds.

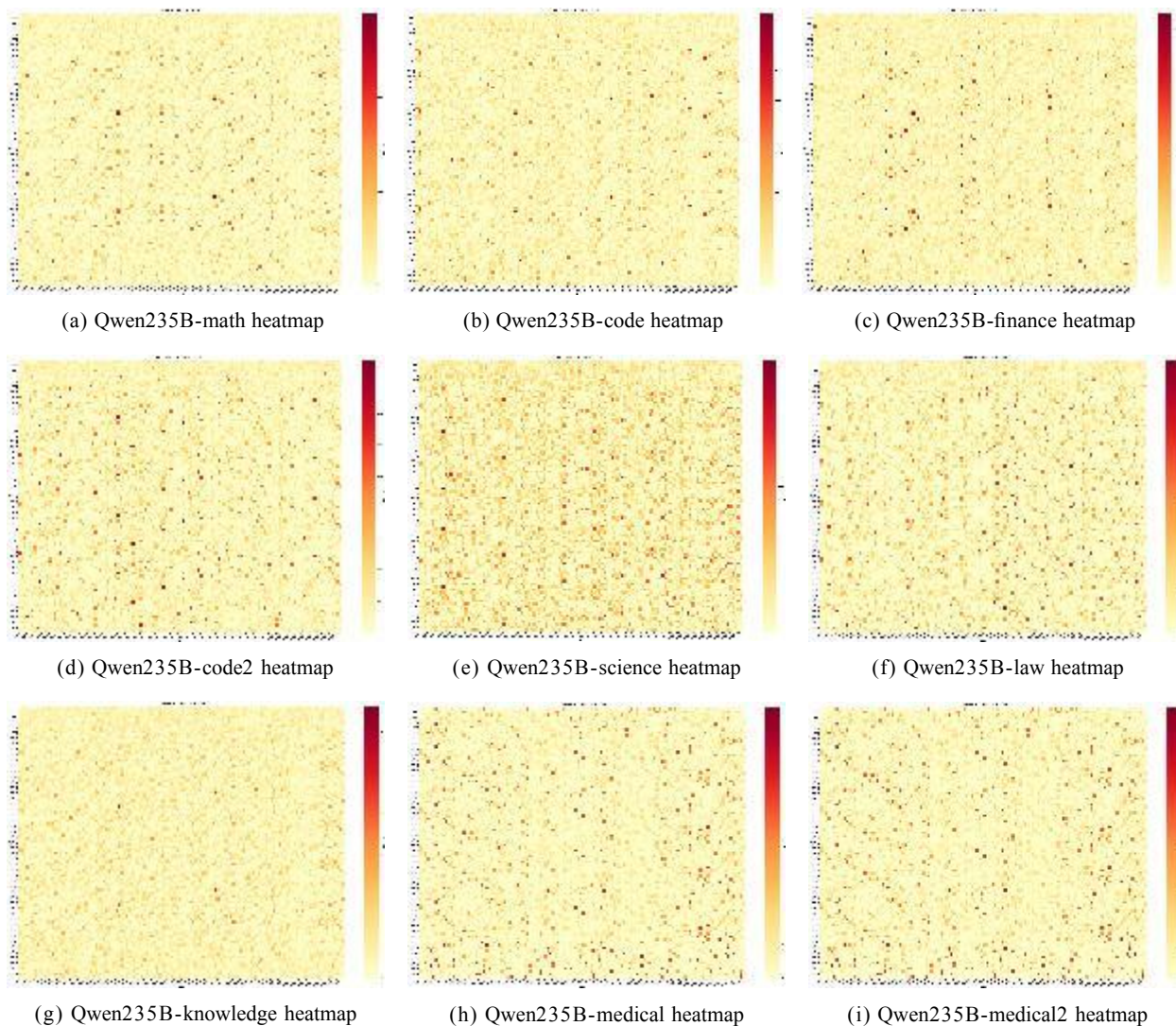


Figure 11: Qwen3-235B-A22B-Thinking model activation. a) Divergent Activation Densities: High-density expert recruitment is observed in science and law, while the knowledge domain exhibits a near-uniform distribution across the manifold, indicating a lack of dominant expert "hotspots." b) Sub-task Bifurcation: Expert selection for Code and Code 2 reveals a clear trajectory shift, reflecting task-specific routing adaptability in high-parameter MoE architectures.

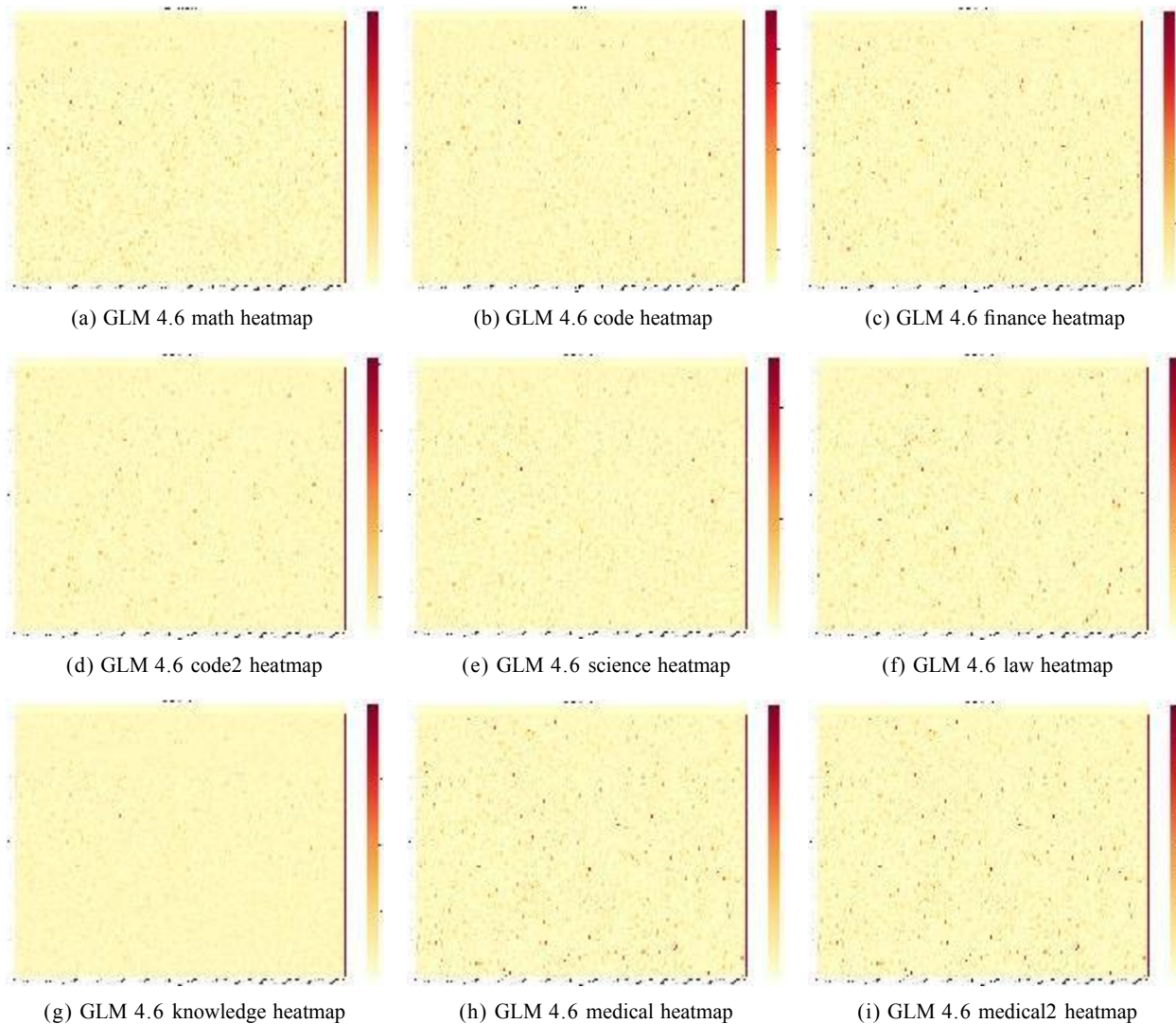


Figure 12: GLM 4.6 model activation. a) Distributed Synergy: The model shows near-uniform expert activation across diverse tasks, suggesting a high-entropy routing approach with minimal cross-domain divergence. b) Selective Expertise: A localized increase in expert recruitment intensity is observed in the medical domain, representing a distinct functional preference within an otherwise homogeneous routing manifold.

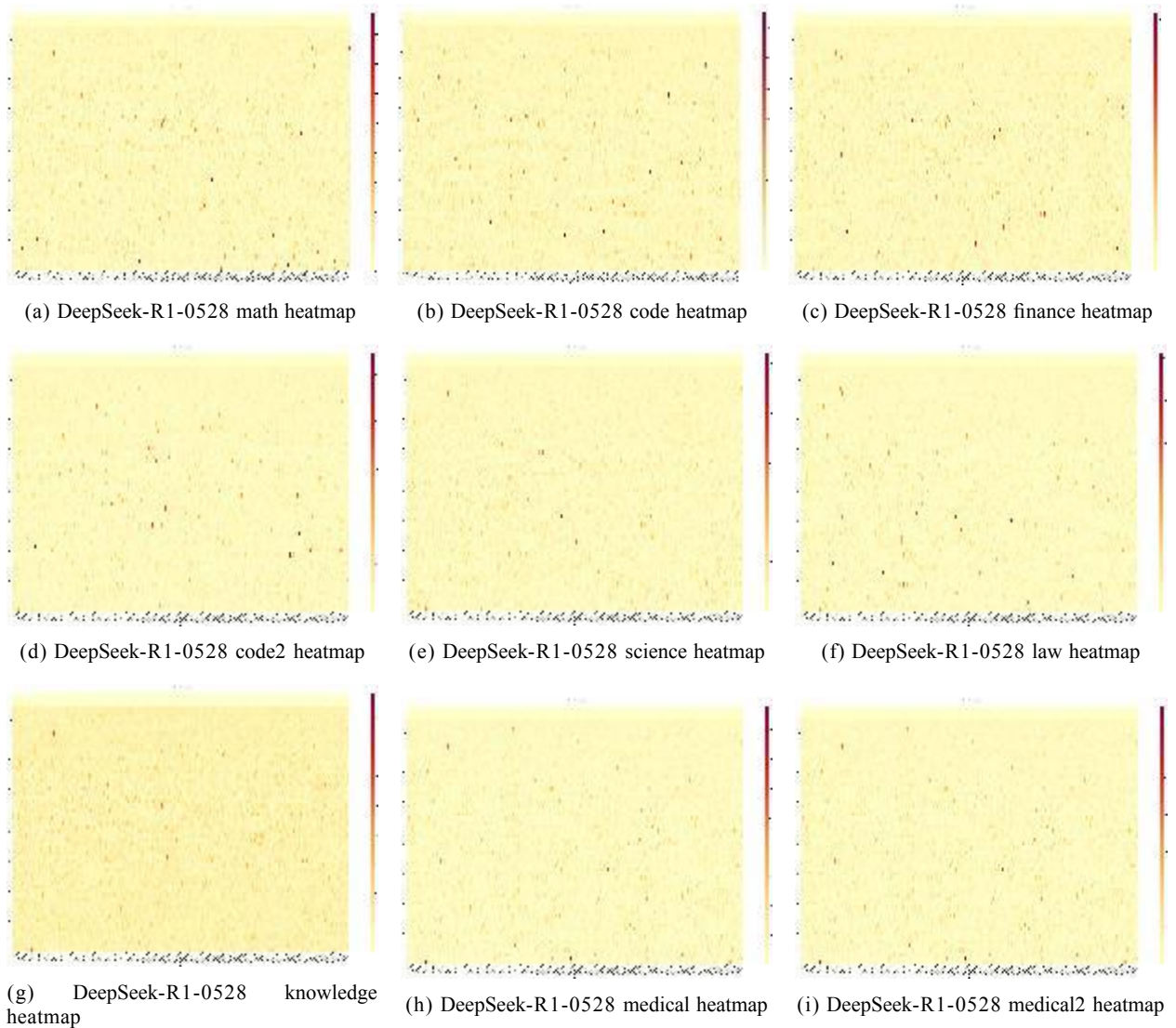


Figure 13: DeepSeek-R1-0528 model activation. a) Distributed Load Balancing: The model demonstrates near-equivalent expert utilization across diverse tasks, indicating a high-entropy routing policy that maintains a balanced expert load. b) Task-Specific Intensity: Pronounced activation "hotspots" appear specifically in the code domain, highlighting a distinct functional preference for programming and logic-heavy contexts within an otherwise homogeneous manifold.

B MoE Specialization and Performance

A specified expert will give the insight of specialized fields, but if the specialty reduce the experts performance, this will make the system collapse thus we analyze the specialty along with performance on some domain benchmarks.

B.1 Theoretical Proof of Error Bound using NGR

First, (author?) have proved using mathematical computation. We apply the findings to Qwen3, GLM and DeepSeek.

Lemma B.1 (Generalization Bound for Sparse MoE). *Let the MoE model be C-Lipschitz and the MLP layers be defined by a neural network function class with a fixed structure S. Given input $\|x^{(0)}\|_2 \leq c$, and weight matrices constrained by spectral norms $\|W_i\|_{\text{op}} \leq K_i$, the generalization error upper bound is:*

$$O\left(4C \frac{c}{\sqrt{m}} \cdot \left(\prod_{i=1}^r K_i\right) \cdot \left(\sum_{i=1}^r \frac{b_i^{2/3}}{K_i^{2/3}}\right)^{3/2} + 2\sqrt{\frac{2kdp^2(1 + \log(\frac{T}{k})) + dp^2 \log(2m) + \log(\frac{4}{\delta})}{2m}}\right). \quad (14)$$

Applying Lemma B.1 to architectures like Qwen3-MoE, GLM and DeepSeek-MoE, we observe that Top-K selection acts as a regularizer. The term $\log(\frac{T}{k})$ explicitly shows that as the total experts T grow relative to selected k , the model requires a logarithmic increase in samples to maintain the generalization gap.

B.2 Benchmark Performance vs. Specialty

We investigate whether structural expertise correlates with the model’s objective performance across diverse reasoning tasks. Table 9 presents benchmark results compiled from official technical reports. While certain benchmarks are domain-specific and lack exhaustive cross-model testing, the current data highlights a significant trend. Notably, DeepSeek-R1-0528 achieves highly competitive results, particularly in specialized domains such as coding, advanced mathematics, and scientific reasoning. These findings support our hypothesis: a high degree of architectural specialization (Expertise) directly translates to superior performance in complex, high-entropy tasks.

Table 9: Comparison of Qwen3, GLM 4.6 and DeepSeek-R1 benchmarks.

ID	Dataset	Q3-32B	Q3-MoE	Q3-235B	GLM	DS-R1	Notes
aime	AIME 2025	72.9%	70.9%	81.5%	93.9%	70.0%	Advanced math reasoning.
CAIS HLE	HLE	8.3%	8%	18.2%	17.2%	17.7%	Extremely difficult 2025 benchmark.
live	LCB	68.4%	62.6%	74.1%	82.8%	68.7%	
swe	SWE-bench	-	-	-	68.0%	57.6%	Verified set.

While Qwen3-30B exhibits competitive specialization, its absolute performance is constrained by its active parameter count. Consequently, we focus our correlation analysis on Qwen3-235B, DeepSeek-R1-0528, and DeepSeek-R1, which possess comparable effective inference capacities (22B-32B active parameters).

Figure 14 demonstrates a robust positive correlation between architectural specialty and task performance, suggesting that superior reasoning capabilities are inherently tied to domain-specific expert grounding. A granular analysis in Figure 15 reveals nuanced relationships between individual metrics and accuracy. Notably, Rademacher Complexity serves as a strong negative indicator ($r = -0.3411(500)$, $-0.3774(1000)$, $-0.2676(2000)$), reinforcing the premise that lower routing complexity (higher determinism) favors model proficiency.

The Stability Paradox. Intriguingly, while most sequence-level metrics align positively with performance, the N-gram ratios for longer windows ($n = 10, 20$) exhibit a surprising inverse correlation ($r = -0.5675$ and -0.6545 , respectively). This divergence suggests two underlying mechanisms:

- **Hierarchical Routing Efficiency:** Top-performing models like GLM-4.6 and DeepSeek-R1 leverage a hierarchical "Group-Expert" strategy. Our results show that while expert-level persistence may fluctuate, the Group N-gram ratio maintains a strong positive correlation (0.6663 for $n = 2$ and 0.6201 for $n = 5$). This implies that the model’s "expertise" is anchored at the group (domain) level, allowing for dynamic expert switching within a stable functional cluster.
- **Impact of Training Constraints:** The prevalence of forced Load-Balancing losses during training across these SOTA models likely induces divergent expert utilization. This pressure to distribute tokens across

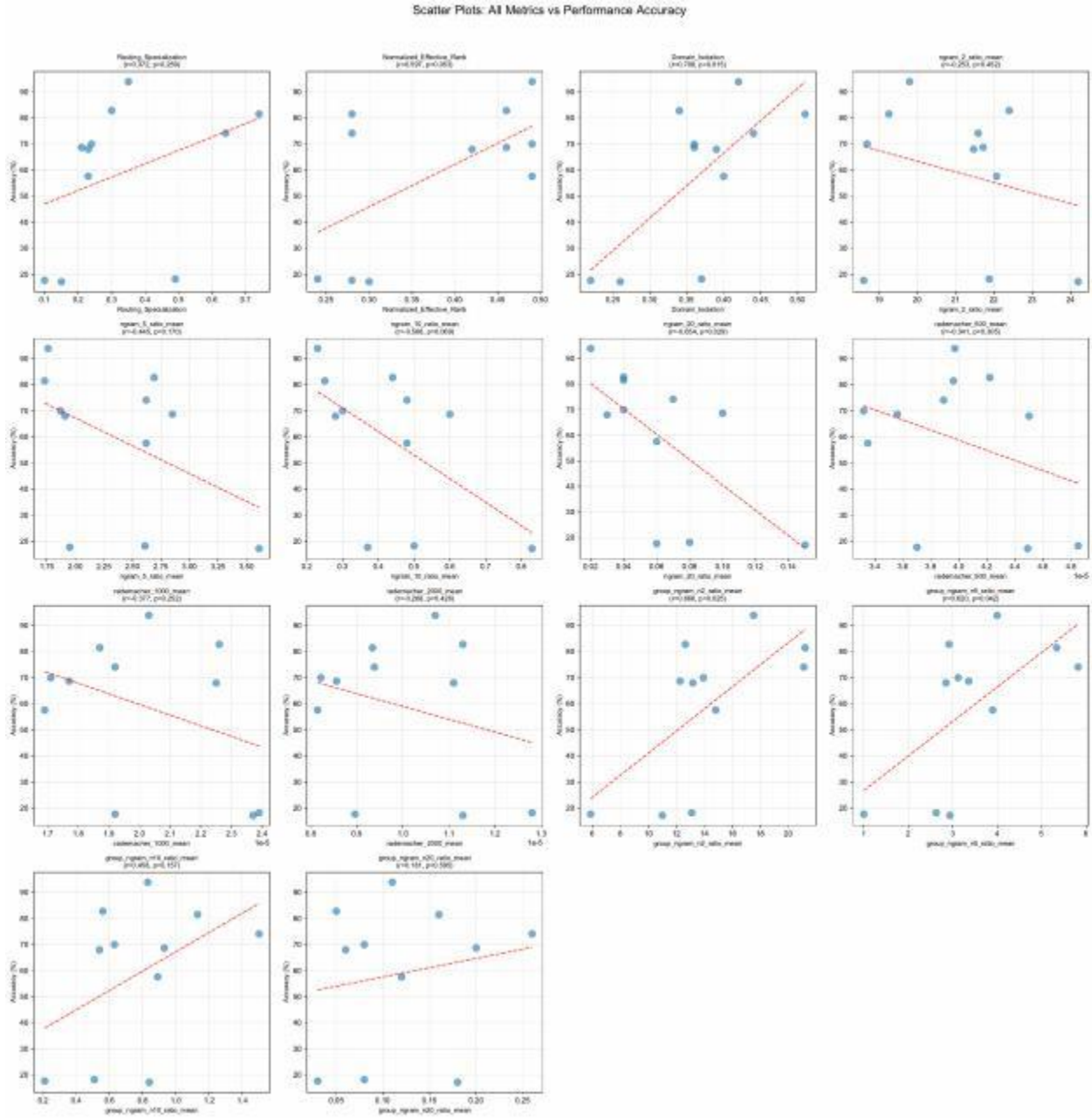


Figure 14: Correlation of Performance with each metric. a) Positive Predictors: Core specialization metrics—including Routing Specialization (S_{spec}), Normalized Effective Rank (R_{eff}), Domain Isolation (S_{iso}), and long-range temporal stability (N-gram ratio-10 and Group N-gram ratio-10)—exhibit a strong positive correlation with model accuracy. This alignment suggests that macroscopic domain-anchoring and sustained expert trajectories are primary drivers of reasoning proficiency. b) Inverse Indicators: Rademacher Complexity and short-range expert transitions (N-gram-2, N-gram-5) show a negative correlation with performance. This inverse relationship indicates that while micro-level expert switching is inherent to the MoE architecture, excessive routing stochasticity and lack of long-range expert commitment (high Rademacher complexity) can be detrimental to specialized problem-solving.

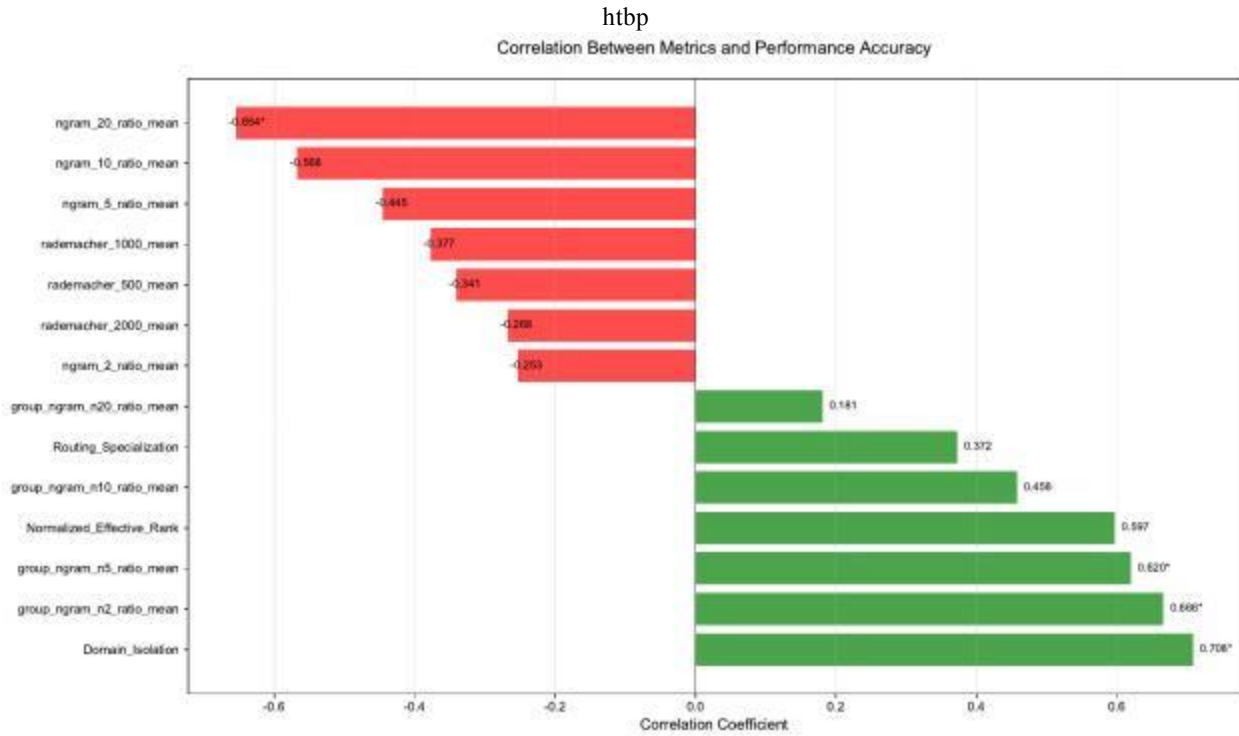


Figure 15: Correlation of Performance with each individual metric. a) Inverse Indicators (Red Bars): Metrics such as Rademacher Complexity and short-range expert transitions ($n = 2, 5$) are negatively correlated with accuracy. This suggests that excessive routing stochasticity and micro-level "expert jitter" act as structural noise that compromises reasoning stability. b) Positive Predictors (Green Bars): Core metrics—including Routing Specialization (S_{spec}), Normalized Effective Rank (R_{eff}), Domain Isolation (S_{iso}), and long-range temporal consistency ($n = 10$)—show a strong positive correlation with performance. These results demonstrate that a specialized, modular, and temporally persistent expert manifold is a fundamental driver of superior model proficiency.

the expert manifold may break long-range expert-level consistency ($n \geq 10$) while preserving macro-level domain specialization.

C N-gram Expertise–Theretical Analysis

C.1 MoE as Bellman Optimization System

C.1.1 Why view MoE as Bellman Optimization

Action Space (A) The decision-maker (router) at each layer l for each sequence index t_i selects a subset of experts $K_{l,t_i} \subset \{1, \dots, E\}$. For a Top-k routing policy, the action at a specific temporal-layer coordinate (l, t_i) is:

$$a_{l,t_i} = K_{l,t_i} \in K \subseteq [E] : |K| = k \quad (15)$$

Transition Dynamics The transition occurs along the depth axis (layer-wise) for each token in the sequence. Let $G : S \rightarrow R^E$ be the gating function and $E_e : S \rightarrow S$ be the e -th expert function. The state evolution for a token t_i from layer l to $l + 1$ is defined as:

$$s_{l+1,t_i} = \text{Trans}(s_{l,t_i}, K_{l,t_i}) = \sum_{e \in K_{l,t_i}} G_e(s_{l,t_i}) \cdot E_e(s_{l,t_i}) \quad (16)$$

This formulation allows the Bellman system to track the "history" of a token's representation as it traverses the expert manifold.

Reward and Policy The policy π dictates the expert selection based on the local hidden state: $\pi(s_{l,t_i}) = \text{arg-TopK}(G(s_{l,t_i}))$. We define the reward $r(s_{l,t_i}, K_{l,t_i})$ as the contribution to the negative differential loss. Crucially, for our specialized RL training plan, we define the Expertise-Augmented Reward:

$$r_{\text{aug}}(s_{l,t_i}, K_{l,t_i}) = r_{\text{task}} + \lambda \cdot l(\text{consistency across } t_{i-n:i}) \quad (17)$$

where the second term explicitly rewards the temporal consistency of expert selection across the n -gram window. **A.1.3 Bellman Operators and Error Matrix**

Sequence-Aware Bellman Operator For a value function $V : S \rightarrow R$, the Bellman operator T^π now operates on the sequence-indexed state:

$$(T^\pi V)(s_{l,t_i}) = r(s_{l,t_i}, \pi(s_{l,t_i})) + \gamma V(s_{l+1,t_i}) \quad (18)$$

where γ is the discount factor representing the decay of influence across layer depth.

Bellman Error Matrix (M) The error matrix M is constructed over the set of observed tokens across the corpus and the set of routing policies Π :

$$M(t_i, l), \pi_\theta = E(s_{l,t_i}, \pi_\theta) = (T^{\pi_\theta} V)(s_{l,t_i}) - V(s_{l,t_i}) \quad (19)$$

The Bellman Rank $\kappa = \text{rank}_\epsilon(M)$ thus measures the complexity of the routing task across both the depth of the model and the temporal structure of the language.

C.1.2 Proof of Low-Rank Structure

Theorem C.1. *If the gating function G and expert functions E_e are Lipschitz continuous, then the Bellman Error Matrix M possesses a low numerical rank κ .*

Proof. Consider the mapping $(s, \theta) \mapsto E(s, \pi_\theta)$.

1. **Lipschitz Continuity:** By assumption, G is C -Lipschitz. Since the transition dynamics and rewards are compositions of G and E_e , the function E is also Lipschitz continuous.
2. **Function Approximation:** For any $\epsilon > 0$, the space of Lipschitz functions over a compact domain can be ϵ -approximated by a finite set of basis functions $\{\psi_i\}_{i=1}^N$.
3. **Matrix Factorization:** Each entry M_{s,π_θ} can be approximated as $\sum_{i=1}^{\kappa} u_i(s)v_i(\theta)$. The number of required components κ scales with the covering number of the function class, which is logarithmic relative to the precision ϵ .

Thus, $\kappa \leq O(d \log \frac{CR}{\epsilon})$, where d is the intrinsic dimension of the representation space. \square

C.1.3 Why Make MoE a Bellman Optimization System

While this paper focuses on the appraisal of existing specialization, the theoretical framework provided by the Bellman Rank and NGR serves as the objective function for a future Reinforcement Learning of Expert Specialization training stage.

Planned Reward Formulation We propose a composite reward signal R_{spec} to be used in post-training to incentivize experts to branch into specialized "tributaries" rather than collapsing into the shared "mainstream" knowledge:

$$R_{\text{spec}} = \alpha \cdot \mathbb{E}_{\text{NGR}}^{(n)} - \beta \cdot \widehat{\mathcal{R}m}(\mathbb{G}_{\theta^*}) \quad (20)$$

where α rewards temporal consistency (expertise) and β penalizes routing noise (complexity).

Implementation Note This RL-based training paradigm is currently in the design phase. The metrics introduced in this work (RS, NER, DI, and NGR) provide the necessary diagnostic tools to verify if such a reward system successfully induces functional isolation without compromising the model's foundational reasoning capabilities.

C.2 MoE with Mutual Information

Proof. The proof proceeds by bounding the probability of the "constant path" event using information-theoretic inequalities.

C.2.1 Mutual Information Decomposition

By the definition of Mutual Information:

$$I(\mathbf{x}_{1:n}; \mathbf{p}_{1:n}) = H(\mathbf{p}_{1:n}) - H(\mathbf{p}_{1:n} | \mathbf{x}_{1:n}) \quad (21)$$

In a learned MoE, the gating policy \mathbb{G} minimizes the conditional entropy $H(\mathbf{p}|\mathbf{x})$ to ensure deterministic expert specialization. Thus, as $H(\mathbf{p}_{1:n}|\mathbf{x}_{1:n}) \rightarrow 0$, the mutual information $I_n(\mathbf{x}; \mathbf{p})$ is lower-bounded by the entropy of the routing distribution $H(\mathbf{p}_{1:n})$.

C.2.2 Entropic Chain Rule and Local Consistency

We expand the joint entropy of the routing path using the chain rule:

$$H(\mathbf{p}_{1:n}) = \sum_{t=1}^n H(p_t | p_{1:t-1}) \quad (22)$$

High $\mathbb{E}_{\text{NGR}}^{(n)}$ implies that the transition probability $P(p_t = p_{t-1} | p_{t-1})$ is high. Let σ denote the event of a consistent path ($p_1 = p_2 = \dots = p_n$). In the manifold of all possible paths $\Pi^{(n)}$, the N-gram Expertise is the empirical measure of this specific subset:

$$\mathbb{E}_{\text{NGR}}^{(n)} = P(\sigma) = \frac{\text{Card}(\omega \in \Omega^{(n)} : p_1 = \dots = p_n)}{\text{Card}(\Omega^{(n)})} \quad (23)$$

C.2.3 Concentration Inequality

Using the relationship between entropy and the probability of the most likely sequence (Fano's inequality variant), we observe that $H(\mathbf{p}_{1:n})$ is maximized when the distribution is uniform. Conversely, a high $I_n(\mathbf{x}; \mathbf{p})$ signifies that the input \mathbf{x} significantly reduces the effective search space of paths. If $I_n(\mathbf{x}; \mathbf{p})$ is large, the router must "lock" onto specific high-probability trajectories. Given that natural language inputs $\mathbf{x}_{1:n}$ exhibit high temporal redundancy (low $H(\mathbf{x}_t | \mathbf{x}_{t-1})$), a router maximizing mutual information will mirror this redundancy in the routing space, resulting in:

$$H(\mathbf{p}_{1:n}) \leq H_{\text{max}} - I_n(\mathbf{x}; \mathbf{p}) \quad (24)$$

C.2.4 Conclusion

Applying the exponential map to the entropy bound and normalizing by the expert manifold volume E^{n-1} , we obtain:

$$\mathbb{ENGR}^{(n)} \propto \exp(-H(p_1 : n)) \geq \frac{1}{E^{n-1}} \exp\left(\frac{I_n(x; p) - H_{\text{max}}}{n}\right) \quad (25)$$

This confirms that the N-gram Expertise is a lower bound on the information-theoretic coupling between inputs and routing decisions. \square

Refined Logic Notes: $H(p|J) \rightarrow 0$: This assumes the router has "learned" its specialty. If the router is random, NGR is low and MI is low. Normalization: The E^{n-1} factor accounts for the fact that there are E^n total paths, but only E possible "constant" paths (e.g., 1 — 1 — 1, 2 — 2 — 2, etc.). The Log-Exp link: This bridges the gap between the bits of information (MI) and the physical count of repeated paths (NGR).

D Data analysis of interlayer moe distribution and expertise – focus on 1st, middle and last layers

D.1 Layer-wise Routing Specialization Trajectories

Figure 17 visualizes the evolution of expert focus with a unified Y-axis scale. Three key topological patterns emerge:

- **Universal Initialization:** All models start with near-zero specialization, confirming a universal "Shared Stem" for domain-agnostic feature extraction in shallow layers.
- **Magnitude Disparity:** A structural divergence is evident—Qwen models adopt a "Specialist" strategy (maintaining $S_{spec} > 1.0$), while DeepSeek and GLM function as "Generalists" ($S_{spec} < 0.6$).
- **Terminal Bifurcation:** The "Low-High-Low" convergence hypothesis holds for standard Instruct models. However, CoT-finetuned models (Fig. 17 b/c) defy this trend, exhibiting a "Terminal Surge" where deep layers are repurposed for highly isolated, domain-specific reasoning.

D.2 Cross-Domain Similarity in Critical Layers

We visualize heatmaps of expert choice similarity between domains at the first, middle, and last layers to track how knowledge sharing evolves.

The heatmaps (Figure 16) reveal two distinct routing strategies. Qwen-235B exhibit an "High-Low-High" pattern for most domains: tasks share the input layer, separate in the middle for specialized reasoning, and re-integrate at the output layer to share a common representation. A notable exception is Qwen’s Medical domain, which remains strictly isolated (similarity about 0.2) from the very first layer. In contrast, DeepSeek-R1 follows a "progressive separation" pattern: it starts with the highest similarity (>0.9) but separates domains continuously layer by layer, ending with distinct boundaries without the terminal re-integration seen in Qwen.

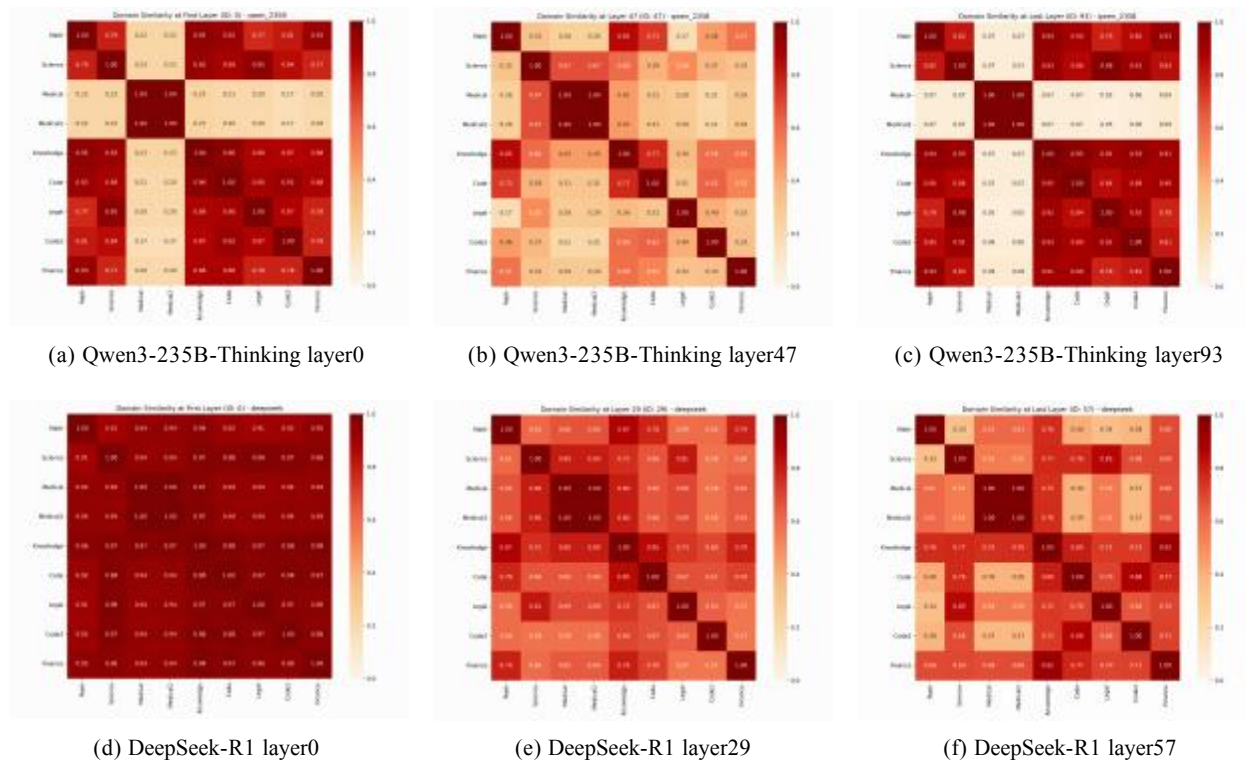


Figure 16: Cross-domain expert similarity heatmaps at initialization, core, and terminal layers. The visualization compares the routing dynamics of (a-c) Qwen3-235B-Thinking and (d-f) DeepSeek-R1. While Qwen demonstrates a "Re-integration" mechanism in the final layer (except for the isolated Medical domain), DeepSeek displays a continuous "Progressive Separation" trend from a unified start to a divergent end.

D.3 Comparative Metrics in Critical Layers

As shown in Table 10, Quantitative analysis of Routing Specialization $S_{spec}^{(1)}$ across critical layers exposes a fundamental divergence in resource allocation strategies. First, at the first layer, Qwen-Thinking models immediately separate the Medical domain (score 0.96), effectively reserving specific experts right from the start. In contrast, DeepSeek and GLM start with almost zero specialization (<0.10), meaning they treat all inputs equally at the beginning. Second, at the last layer, the "Thinking" training causes Qwen to become extremely specialized for complex tasks like Medical (score soaring to 1.90), much higher than its Instruct version (0.82) or other models (0.7). This suggests that Qwen’s "Thinking" process relies greatly on dedicating the final layers to specific hard problems, whereas DeepSeek maintains a more balanced approach throughout.

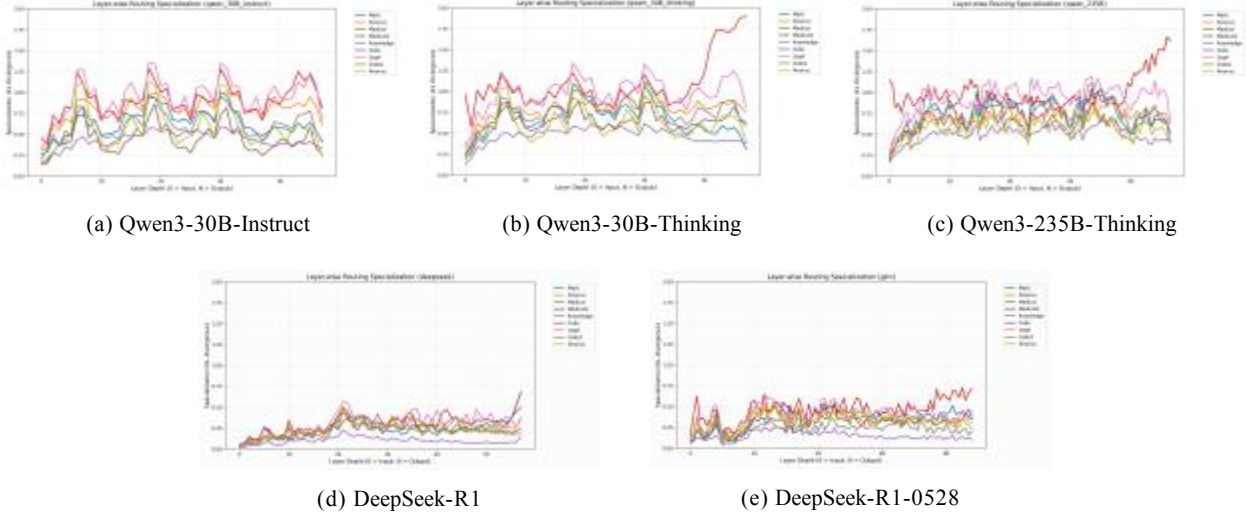


Figure 17: Layer-wise routing specialization (S_{spec}). (a, d, e) Standard models (Instruct/Base) follow a convergence pattern, declining in final layers for feature integration. (b, c) CoT-finetuned models exhibit a distinct "Terminal Surge", sustaining high specialization for reasoning. Note the magnitude gap: Qwen architectures show significantly stronger expert isolation compared to DeepSeek and GLM.

Table 10: Routing Specialization (S_{spec}) across critical layers.

MODEL	LAYER	MATH	SCIENCE	MEDICAL	MEDICAL2	KNOWLEDGE	CODE	LEGAL	CODE2	FINANCE
QWEN3-30B-INSTRUCT	LAYER 0	0.27	0.31	0.45	0.45	0.15	0.15	0.33	0.21	0.16
	LAYER 24	0.68	0.82	0.85	0.85	0.54	0.35	0.96	0.58	0.46
	LAYER 47	0.41	0.61	0.82	0.82	0.33	0.26	0.67	0.42	0.23
QWEN3-30B-THINKING	LAYER 0	0.19	0.31	0.96	0.96	0.13	0.25	0.36	0.22	0.20
	LAYER 24	0.76	0.86	0.85	0.85	0.62	0.62	0.98	0.78	0.53
	LAYER 47	0.31	0.76	1.90	1.89	0.39	0.63	0.81	0.59	0.40
QWEN3-235B-THINKING	LAYER 0	0.30	0.30	0.69	0.69	0.26	0.26	0.31	0.32	0.32
	LAYER 47	0.55	0.52	0.57	0.57	0.42	0.51	0.67	0.60	0.60
	LAYER 93	0.33	0.32	0.81	0.81	0.28	0.32	0.33	0.32	0.33
DEEPSEEK-R1-0528	LAYER 0	0.06	0.05	0.06	0.06	0.02	0.03	0.05	0.03	0.03
	LAYER 29	0.22	0.29	0.31	0.32	0.12	0.19	0.28	0.26	0.28
	LAYER 57	0.50	0.38	0.68	0.68	0.15	0.25	0.35	0.19	0.18
GLM-4.6	LAYER 0	0.09	0.11	0.15	0.15	0.05	0.10	0.11	0.08	0.09
	LAYER 44	0.43	0.41	0.49	0.49	0.19	0.39	0.58	0.37	0.44
	LAYER 88	0.37	0.31	0.72	0.72	0.10	0.35	0.45	0.20	0.21

E DBES: Domain Bench of Expert Specialty

Detailed database statistics is shown in Table 11 and the whole database is on Huggingface.

Table 11: Domain Bench of Expert Specialty(DBES)

Partition	Domain	Samp.	Source	Type
AIME 2025	Math	30	(author?) [23]	Logical Reasoning
AllenAI SciQ (Val)	Science	1000	(author?) [24]	Scientific Knowledge
BigBio MedQA (Dev)	Medical	1623	(author?) [25]	Professional Exam
BigBio MedQA (Test)	Medical2	1815	(author?) [25]	Professional Exam
CAIS HLE	Knowledge	1,600	(author?) [26]	Multi-subject Knowledge
LiveCodeBench (Test)	Code	400	(author?) [27]	Code Generation
Nguha LegalBench	Legal	1,600	(author?) [28]	Legal Reasoning
Princeton SWE-bench (Test)	Code2	500	(author?) [29]	Software Engineering
Yale-FinanceMath (Val)	Finance	200	(author?) [30]	Financial Math

F Alternative Perspectives on Specialization versus Generalization

In this paper, we emphasize the specialization of MoE models, but we could not ignore the problem of exploring generalized artificial intelligence. Thus, we explore the tension and balance between specialization and generalization in machine learning models from diverse viewpoints in this part.

F.1 The Human Understanding of Knowledge Hierarchies

In human cognition, knowledge is not stored in isolation but is organized into complex, hierarchical structures—often conceptualized as "knowledge trees." This framework comprises:

- **A Broad Foundational Base (General Knowledge):** This includes fundamental logic, common sense, and cross-domain principles (e.g., mathematics, physical laws). These elements form the foundational framework for understanding and learning new concepts.
- **Deep, Specific Branches (Specialized Knowledge):** These are detailed, refined clusters of knowledge within specific domains (e.g., medicine, law, programming). They depend on the foundational base and are densely interconnected with other branches within the same domain.
- **Dynamic Growth and Interconnection:** New knowledge can either deepen an existing branch (specialization) or create novel connections between different branches, leading to interdisciplinary insights—a form of advanced generalization.

The development of a human expert typically involves progressing from a broad, general education to increasing depth within a chosen branch. This structure suggests that genuine "intelligence" may require a similarly scalable and deepenable hierarchical knowledge architecture.

F.2 The Imperative for Generalization in Large Language Models

For Large Language Models (LLMs), robust generalization capability is a core value and fundamental necessity, primarily due to the following reasons:

- **Handling Open-Domain Tasks:** The distribution of real-world problems and queries is immensely wide. Models must comprehend and respond to topics, phrasings, or task combinations not explicitly seen during training.
- **Functioning as Foundational Models:** Their intended role is often as a starting point for downstream applications. Broad coverage and basic competencies in logic and language understanding (generalization) enable rapid adaptation to diverse specific needs via lightweight methods like fine-tuning or prompt engineering.
- **Fostering Emergent Abilities:** Many complex reasoning, analogical, and creative capabilities often "emerge" only after a model achieves sufficient scale and breadth of general knowledge. Premature overspecialization can potentially stifle this latent potential.

Thus, generalization ensures a model's flexibility, robustness, and viability as a foundational platform.

F.3 The Value of Specialization for Downstream Applications

While generalization provides the foundation, specialization is crucial for translating model capabilities into practical value:

- **Enhancing Accuracy and Reliability:** In high-stakes domains like healthcare, law, or finance, model outputs must adhere to highly specialized norms, terminology, and factual standards. Specialized fine-tuning significantly reduces domain-specific "hallucinations" and commonsense errors.
- **Optimizing Efficiency and Cost:** A model optimized for a specific task (e.g., customer service, code generation) typically offers faster inference, lower computational resource requirements, and a more precise understanding of domain-specific intent.
- **Enabling Deep Integration:** Specialized models can more effectively understand and invoke domain-specific tools, APIs, or databases, becoming seamless automated components within professional workflows.
- **Meeting Compliance and Security Requirements:** Industry-specific standards for data handling, security, and auditability are often best addressed through controlled and verifiable specialized model versions.

